Enrichment of Volcanogenic Trace Elements in a Continuous Subsurface Eagle Ford Core in South Texas and the Origin of The Oceanic Anoxic Event II at The Cenomanian-Turonian (C/T) Boundary

by

DANIEL VALENCIA

Presented to the Faculty of the Graduate School of

The University of Texas at Arlington in Partial Fulfillment

of the Requirements

for the Degree of

MASTER OF SCIENCE IN GEOLOGICAL SCIENCES…..

THE UNIVERSITY OF TEXAS AT ARLINGTON

August 2017

Acknowledgements

Firstly, I would like to express my sincere gratitude to my advisor Prof. Asish Basu for the continuous support of my M.S. study and related research, for his patience, motivation, and immense knowledge. His guidance helped me in all the time of research and writing of this thesis.

Besides my advisor, I would like to thank the rest of my thesis committee: Prof. Andrew Hunt and Dr. Matthew Loocke, for their insightful comments and encouragement, but also for the question which incented me to widen my research from various perspectives.

My sincere thanks also goes to Dr. Loocke who provided me an opportunity to conduct research, and who gave access to his laboratory and research facilities. Without his support it would not have been possible to complete this study.

I thank my fellow labmates for the stimulating discussions, for the long nights we were working together before deadlines, and for all the good memories we have shared in the past three years.

Finally, I must express my very profound gratitude to my family for providing me with unfailing support and continuous encouragement throughout my years of study and through the process of researching and writing this thesis. This accomplishment would not have been possible without them. Thank you.

August 30, 2017

Abstract

Enrichment of Volcanogenic Trace Elements in a Continuous Subsurface Eagle Ford Core in South Texas and the Origin Of The Oceanic Anoxic Event II at The Cenomanian-Turonian (C/T) Boundary

Daniel Valencia, MS

The University of Texas at Arlington, 2017

Supervising Professor: Asish Basu

The Upper Cretaceous Eagle Ford Shale of South Texas is a dark grey to black, sporadically laminated, organic rich carbonaceous mud rock located in the subsurface (~13,000), of the hydrocarbon producing shale-oil formation. This black shale formation was deposited contemporaneously worldwide across the Cenomanian-Turonian (C/T) boundary and records the Oceanic Anoxic Event (OAE-II).

Geochronological and geochemical analysis of a ~300ft long continuous South Texas Eagle Ford Shale core was conducted to further constrain the sub-surface nature of the formation. Major, minor and trace element concentrations were analyzed by ED-XRF to characterize the local geochemical heterogeneity in the formation. Total Organic Carbon (TOC), $\delta^{13}C$ and $\delta^{18}O$ analysis were carried out to constrain and correlate the recorded Oceanic Anoxic Event II (OAEII) in the core.

Volcanic ash beds were sampled at the top and middle of the Eagle Ford and by mineral separation yielding abundant non-detrital zircons for geochronological dating. The U-Pb zircon ages agree with the top of the Eagle Ford and with the inferred middle Eagle Ford, (C/T) boundary. Using this horizon, the onset of OAE2 can be further constrained and correlated with the positive $\delta^{13}C$ excursion.

With a definitive constraint for OAE2 established, this key interval was analyzed at a higher resolution using Energy Dispersive X-ray Fluorescence (ED-XRF). The high-resolution sampling of the core shows ~80-99% increase in concentrations of Cr, Cu, Ni, Mo and Zn over the average Post Australian Archean Shale(PAAS), representative of average continental crust. These findings show significantly increased volcanogenic trace metal input correlating with increased TOC and positive $\delta^{13}C$ values at the C/T dated zircon horizon. These volcanogenic-rich intervals reach peak values before the onset of OAEII and at the maximum values for the positive $\delta^{13}C$ isotope excursion directly after the C/T inferred ash bed. Extensive research has been conducted to construct a robust stratigraphic framework to present a better understanding in the timing and nature of the conditions present during the deposition of the Cenomanian-Turonian Eagle Ford Shale of South Texas.

Table of Contents

List of Illustrations

Chapter 1

INTRODUCTION

1.1 Background

'Black shales' of the Cretaceous period, are characteristic of episodic, contemporaneous deposition of globally distributed organic-rich, carbonaceous marine sediments (Jenkyns, 1980). The dark grey to black, laminated, black shales gained both geologic and economic attention when they were recognized as potential source rock for petroleum and natural gas in mid-1900's (Schlanger and Jenkyns, 1976; Arthur and Schlanger 1979). These Cretaceous episodic periods of black shale deposition were defined by (Schlanger and Jenkyns, 1976) as Oceanic Anoxic Events (OAEs), major global perturbations in the carbon cycle that prompted oxygen deficient oceanic bottom waters resulting in reducing conditions and the preservation of enhanced organic carbon burial.

The stratigraphic framework of OAEs first developed from field observations of on-land outcrops found in a variety of paleo-depositional settings including oceanic plateaus and basins, continental margins and shelf seas (Jenkyns, 1980). The Deep-Sea Drilling Project (DSDP), initiated in the 1970's, and subsequent ocean drilling programs played a vital role in advancing the study of Cretaceous OAEs by collecting fresh black shale samples from previously unsampled ocean basins (ie. Atlantic, Indian, and Pacific oceans)(Ohkouchi et al., 2015). One of the most significant findings from the drilling programs showed the Cretaceous oceans to be key sites of marine-deposited sediments anomalously enriched in organic carbon, 'black shales'. The discovery of the widespread nature of black shale deposits suggested that they were not strictly controlled by local basin geometry but rather complex climatic control on influx of organic matter and sediment, rates of upwelling, sea surface production of organic matter, and preservation

of organic matter related to deep water dissolved oxygen concentration (Walter and Dorrik, 1984,).

One of the most prominent global perturbations in the carbon cycle occurred in the Upper Cretaceous epoch at 100-66Ma. Scholle and Arthur (1980), noted that marine strata deposited at or very close to the Cenomanian-Turonian (C/T) boundary (93.6 ± 0.60 Ma; Kowallis (1995), was uncommonly rich in dark-grey to black, pyritic, laminated shales with total organic carbon (TOC) contents ranging from between 1 and 2% to greater than 20% which is largely of marine planktonic origin. The general lack of bioturbation throughout the boundary interval indicated an absence of burrowing fauna, evidence of anoxic conditions. Although in the coeval pelagic and shelf limestone sections, the dark shales were often lacking, the C/T boundary was still marked by an increase in $\delta^{13}C$ values of + 2.0% to + 3.0%. The elevated $\delta^{13}C$ values indicated an enrichment of the global ocean in ^{13}C values because of the preferential extraction of ^{12}C by marine plankton, the organic components of which were not recycled back into the oceanic reservoir during this period of enhanced organic-carbon burial (Schangler et al., 1987).

This positive carbon isotope excursion (CIE) was globally recognized as a geochemical marker for the lower boundary of the Turonian, previously defined by the first appearance datum of the ammonite species, *Watinoceras coloradoense* Zone, from the Greenhorn Formation in Colorado. The OAEII spans the Cenomanian Turonian boundary event which recorded one of the ten most severe biotic disasters in the geologic record with the extinction of approximately 26% of marine animal genera (Raup and Sepkoski, 1986). OAEII has been considered the major cause of the C/T boundary mass extinction(Kauffman and Hart, 1995), however several studies questioned the extent, of this mass extinction (Corfield et al., 1990; Gale et al., 2000; Smith et al. 2001).

Previous studies have also shown that the C/T boundary have recorded the highest eustatic sea-level change of the Mesozoic era (Haq et al., 1988). However, large-scale cycles of sea-level change can and do alter the ratio of shallow to deep marine continental-shelf deposits preserved in the rock record both regionally and globally, possibly showing biases in the rock record (Smith et al., 2001).

Over the past four decades, researchers have conducted detailed studies and integrated biostratigraphically, geochemical, petrological and geochronological methods to try to decipher the enigmatic trigger that initiated the OAEII and the subsequent C/T boundary event. Proposed hypotheses for initiation of global anoxia and enhanced carbon sequestration includes long-term triggers such as changes in ocean circulation and eustatic sea level rise, flooding large areas of continental shelves, promoting global stratification and stagnation in greenhouse climates (Erbacher et al., 2001). Evidence also suggest abrupt episodes of volcanogenic activity and emplacement of Large Igneous Provinces (LIPs) (Orth et al., 1993; Snow et al., 2005; Turgeon and Creaser, 2008; Kuroda et al., 2007) released large quantities of CO_2 into the atmosphere and increased the delivery of hydrothermally derived and weathered nutrients into the photic zone, enhancing primary production (see e.g. Adams et al., 2010). However, recent global studies shows that not all C/T (OAEII) age formations reflect the deposition of organic-rich sediment, therefore suggesting a strong dependence on local and regional processes controlling, sediment input, water stratification basin restriction, bottom currents (Trabucho Alexandre et al., 2010).

The shallow epicontinental Cretaceous Western Interior Seaway (KWIS) (Figure 1), has shown to contrast other globally recognized sections that recorded the organic rich sediment interval during the OAEII (e.g. Plenus Marl and Borelli intervals in

Europe)(Figure 2). Parts of the KWIS have recorded relatively low organic rich and relatively oxygenated sediments in south Texas (Eldrett et al., 2014).

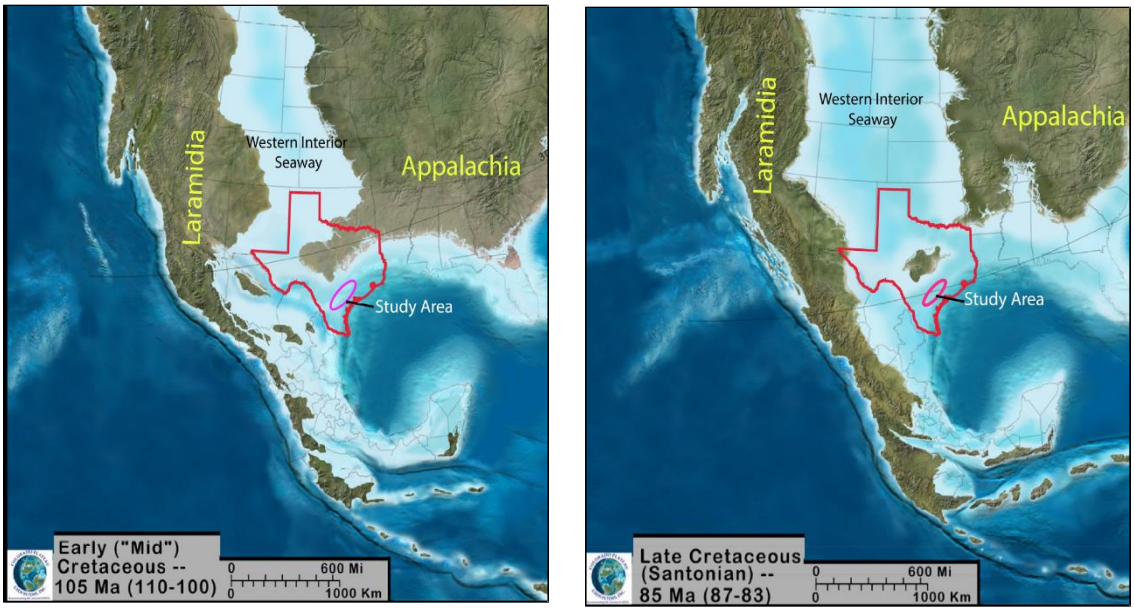

Figure 1.1 Paleogeographic illustration of the KWIS from 105Ma to 85Ma

Modified from Blakely (2013) and Darmaoen (2013)

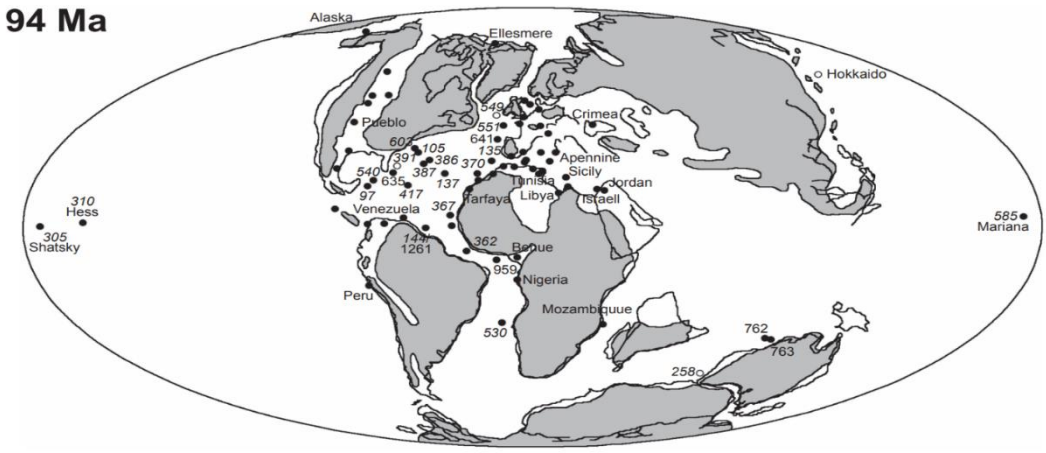

Figure 1.2 World map showing the geographic distribution of black shales formed during OAEII including surface outcrops, subsurface wells and deep ocean drilling sites.

Modified from Ohkouchi (2015).

Recent studies have drawn attention to OAEII time equivalent formations deposited across the southern portion of the KWIS during the (C/T) transition. The intra-shelf basin-carbonate platform conditions were ideal for the preservation of mudstones, limestones and bentonite (weather volcanic ash) beds throughout the Late Cretaceous. The need to progress research of deeply buried subsurface cores from the South Texas Eagle Ford formation is necessary due to the limited knowledge of Late Cretaceous characteristics of the “black shales” deposited during the (C/T) boundary and OAEII

This study aims to constrain a ~300ft long continuous subsurface core using geochronological and geochemical data to reconstruct the oceanic environment at the time of its formation. This localized study area facilitates a better understanding of *in situ* depositional factors that controlled the anoxic bottom water and substantial burial of organic carbon at the OAEII, (C/T) extinction boundary.

1.2 Economic Importance

Organic rich shales have accrued economic importance over the past decade due to technological advances in horizontal drilling coupled with large-scale, multi-stage hydraulic fracturing techniques which have facilitated the production of vast quantities of oil and natural gas previously thought to be impossible or not economically feasible to produce. With the sharp growth in economically driven exploration of organic-rich, black shale formations, new geochemical proxies have been proposed to correlate highly productive, kerogen-rich horizons (sweet spots) throughout the formation.

Although various organic-rich shale plays, (e.g., the Barnett and Haynesville) are currently being explored and exploited in the state of Texas, the (C/T) Eagle Ford Shale (EFS) of South Texas continues to garner attention. The relatively higher carbonate and lower clay percentages of the EFS facilitate a more brittle, ‘frackable’ and economically

viable reservoir (Texas RRC, 2017). The EFS was deposited across the Cenomanian Turonian boundary and records the OAEII (Schlanger and Jenkyns, 1976; Jenkyns et al., 1990).

As of 2015, the most viable energy source in the United States was fossil fuels, accounting for 81.5% of total U.S. energy consumption (U.S. EIA Outlook Annual Energy, 2016), hence, it is vital to progress our understanding of the sedimentological and petrophysical characteristics in hydrocarbon and natural gas-bearing formations. However, the EFS production peaked out around 1.75 million barrels per day (bpd) (Figure 1.3) in early 2015.

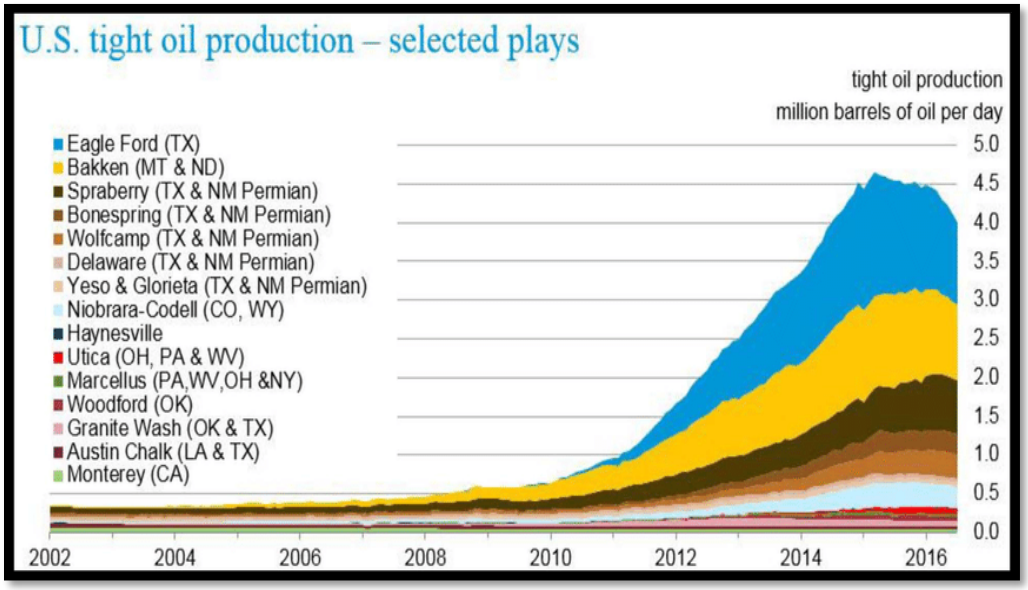

Figure 1. 3 U.S. tight oil production growth from 2008-2015 during “US Shale Oil Boom”. From the U.S Energy Information Administration (EIA), 2016.

After the 2015 peak, the oil and gas price down-cycle or “oil bust” saw EFS production drop by ~approximately 40% to slightly over 1million bpd (U.S. Energy Information Administration 2015). History suggests that oil production is cyclical evidence

by past boom and bust cycles in the industry. Consequently, it seems vital to proceed with continuous geologic research to better understand the processes that influence the lithological variability of US tight oil shale formations like the (C/T) EFS of South Texas. As of July 2017, the EFS has begun to see slight growth in production compared to June 2017 (Figure 1.4), solidifying the importance for prospective research.

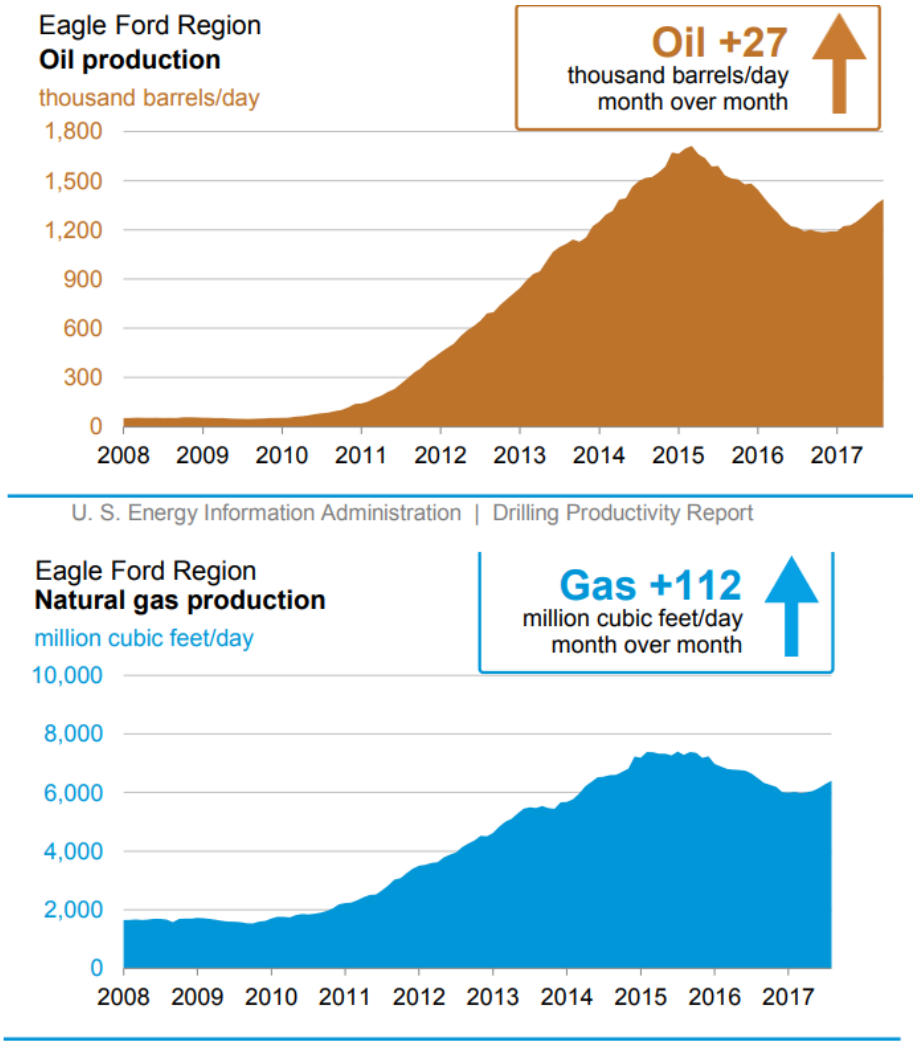

Figure 1.4 Eagle Ford Shale (2008-2017) oil and natural gas production. Monthly productivity report from June 2017 to July 2017.

From the U.S Energy Information Administration (EIA), 2017.

Current Eagle Ford production windows are shown in (Figure 1.5), where the gas window was initially mapped in the Hawkville trend between the Stuart City (Edwards Margin) and Sligo Margin. Production in the oil window was established in 2009 when the oil leg of the Eagle Ford was discovered by EOG Resources, Inc. (Cherry, 2011). The unconventional source rock must go through a set of burial, thermal maturation and petroleum generation conditions to form an organic rich, self-sourcing reservoir. Unconventional reservoirs, like the EFS, typically have lower porosity and permeability compared to conventional wells and, therefore, must be stimulated in some manner (e.g. “fracking”) to enhance the interconnectivity of pore spaces for extraction of hydrocarbons.

The EFS is of interest because the apparent dark-colored, fine-grained, organic-rich sediments comprising the subsurface core have shown geochemically heterogeneous facie. The oil and gas industry has integrated the analysis of chemical variations within sedimentary sequences to determine stratigraphic relationships between visually homogenous rock layers.

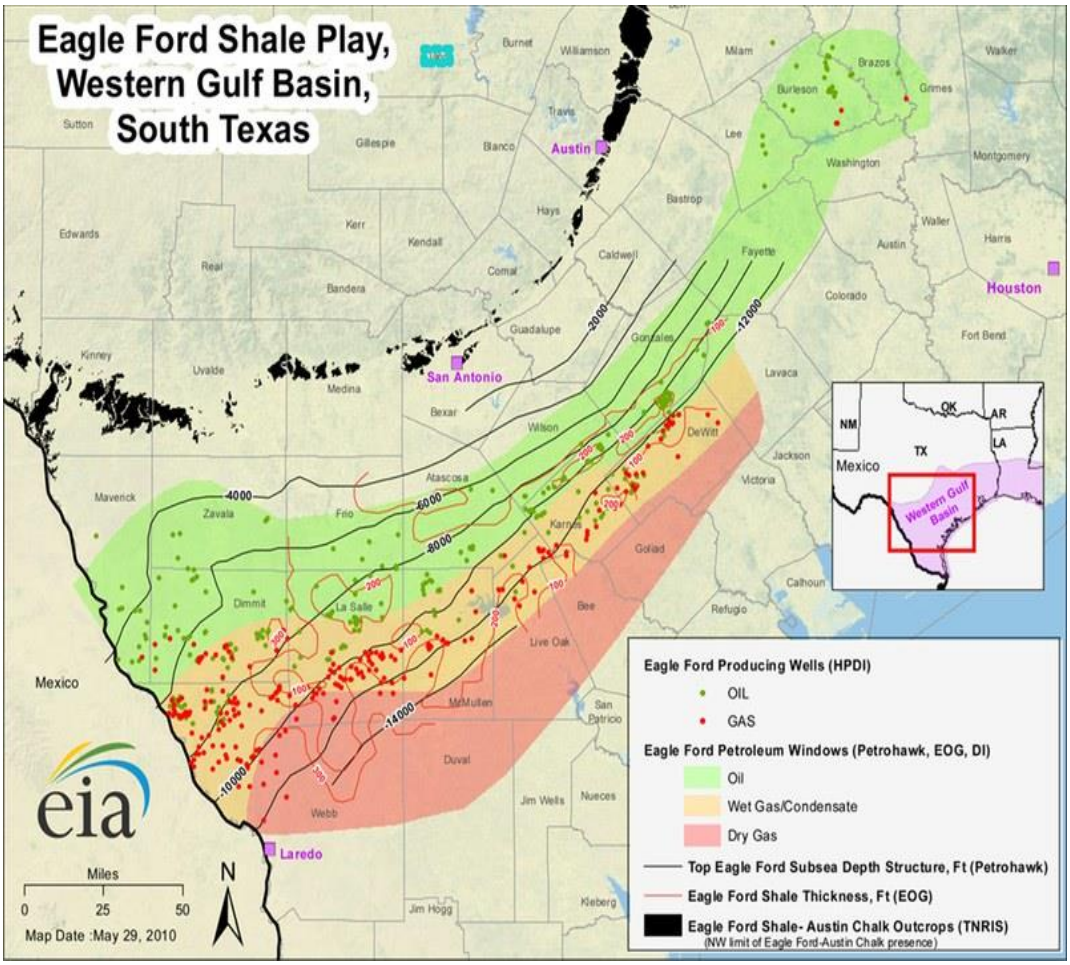

Figure 1.5 Oil, Wet Gas/Condensate and Dry Gas Windows and Producing Wells

Modified from the U.S Energy Information Administration (EIA), 2016.

1.3 Project Objectives and Approaches

The objective of this thesis is to conduct a geochronological and geochemical investigation of a subsurface core to yield insight into possible paleo-depositional conditions responsible for the episodic, contemporaneous widespread deposition of organic carbon-rich black shales seen in the EFS.

This study aims to use a multi-proxy approach to characterize, interpret and correlate the subsurface (C/T) EFS of South Texas. Major, minor and trace elemental concentrations analyzed by energy dispersive x-ray fluorescence (ED-XRF) help to characterize local geochemical heterogeneity within the formation. Total Organic Carbon, $\delta^{13}C$ and $\delta^{18}O$ analysis help to constrain and correlate the recorded global geochemical signature of the OAEII in the core. Volcanic ash beds yielded abundant non-detrital zircons and helped to constraint the inferred C/T boundary. By comparing the results to previous research and modern analogues, the ratios can be used to approximate the (i) sources of organic matter, (ii) rates of paleo-productivity and (iii) help draw a parallel to the positive $\delta^{13}C$ excursion seen globally in stratigraphically equivalent formations.

By utilizing the afore mentioned strategies, a comprehensive assessment of the most widespread and best defined OAE of the mid-Cretaceous will be constructed on a previously inaccessible subsurface EFS core.

The principal approaches in this research are outlined below:

- U-Pb geochronological analyses of single zircon grains from a bentonite bed near the inferred C/T boundary and at the Austin Chalk contact, help to constrain the depositional age of the OAEII and the C/T extinction boundary.
- Select major, minor and trace elemental concentrations coupled with TOC values provide a diverse range of proxies that help define major lithographic facies, paleo-productivity and paleo-redox conditions in the subsurface core.
- Isotope ratios of organic carbon ($\delta^{13}C$) found the strata coupled with T.O.C. and supplementary $\delta^{13}C_{inorg}$, $\delta^{18}O$ to help define the onset of OAEII and assist in constraining and correlating the localized geochemical signatures seen in the core to global findings
- The above approaches support a strong volcanic signature in the rock record of the Eagle Ford Formation of south Texas and its impact on oceanic anoxic conditions.

1.4 Study Location

The Eagle Ford Formation and time equivalent sediments are predominantly found in the subsurface and outcrop as a continuous unit that spans across the state of Texas in a NE - SW direction (Figure 1.6).

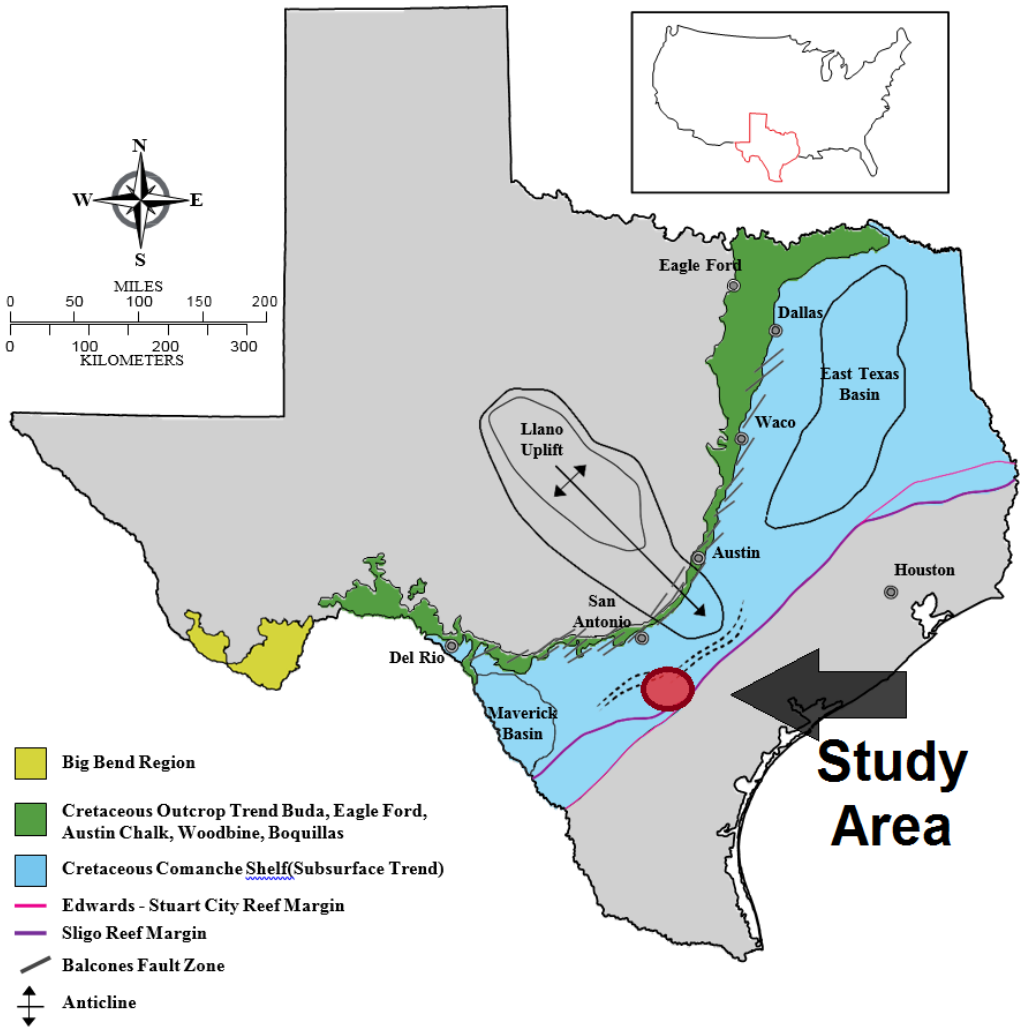

Figure 1.6 Map showing distribution of stratigraphic equivalent Eagle Ford rocks in outcrops and the subsurface of Texas.

Modified from Geology of Texas Map (1992) and Harbor (2011)

The area of study is subsurface and is deposited along the strike of the Lower to Mid-Cretaceous shelf edges, and at times, between the Edwards/Stuart City and Sligo shelf margins. The Edwards/Stuart City and Sligo reef margins are separated by a maximum distance of thirty miles and converge to the northeast near Live Oak and Bee counties; this created an accommodation space and depocenter for a thick package of Eagle Ford sediments (Phelps, 2011).

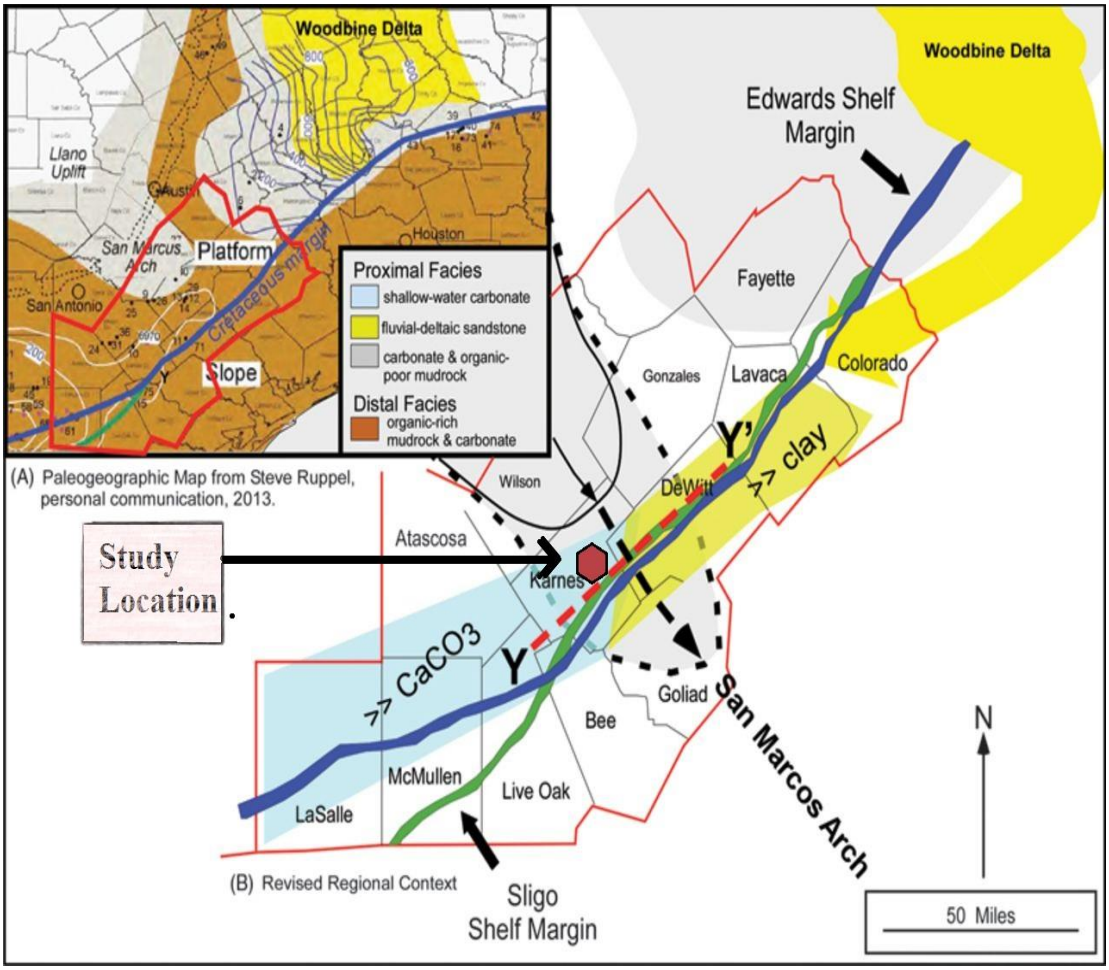

Figure 1.7 Regional Eagle Ford paleogeographic map showing study location relative to San Marcos Arch and Woodbine Delta with study location in red Modified from Bodziak, 2014

The 300ft thick, continuous, subsurface core taken from the study area is located approximately ~13,000ft below the surface on the Comanche Platform directly above the older Edwards/Stuart City and Sligo reef margins. The core is located SW of the San Marcos Arch topographic high and its relative position to the arch provides a barrier that restricted terrestrial clays to the northeast which is observed to produce difficulties in well completions (Bodziak, 2014) (Figure 1.7).

Lithologic heterogeneity of the Eagle Ford Formation in South Texas arises from the mixing of extrabasinal grains of siliciclastic composition with intrabasinal grain assemblages composed dominantly of marine carbonate with a lesser component of bio siliceous debris (Milliken, 2016). The detrital quartz is derived from both extrabasinal and intrabasinal sources, posing a challenge for the use of bulk compositional data for mudrock classification on a regional scale. However, the extrabasinal detrital quartz supplied along a major axis of siliciclastic influx, from the Woodbine depositional system of East Texas, is significantly reduced to a minor part of the grain assemblage in South Texas (Figure 1.7). The lack of input from Woodbine delta sediments to the localized study area facilitates a better understanding of the *in situ* depositional factors that controlled the anoxic bottom water and substantial burial of organic carbon at the OAEII, (C/T) extinction boundary (Bodziak, 2014).

Chapter 2

GEOLOGIC SETTING

2.1 History

The Eagle Ford Group (also called the Eagle Ford Shale (EFS)) is a sedimentary rock formation deposited during the Cenomanian and Turonian ages of the Upper Cretaceous over much of the modern-day state of Texas. The EFS is located in the Western Gulf Basin and was discovered by Ferdinand von Roemer in 1852 and later named in 1887, by R.T. Hill after the town of Eagle Ford, near Dallas, Texas (Hill, 1901).

In 2008, the first well targeting the EFS was drilled by Petrohawk in LaSalle County, Texas. By integrating the innovative horizontal drilling and hydraulic fracturing techniques developed to reach and extract oil and gas from the shale formation (Harbor, 2011). Prior to this time, the Eagle Ford was considered to only be the source rock for the underlying Austin Chalk reservoir(Figurer 2.1).

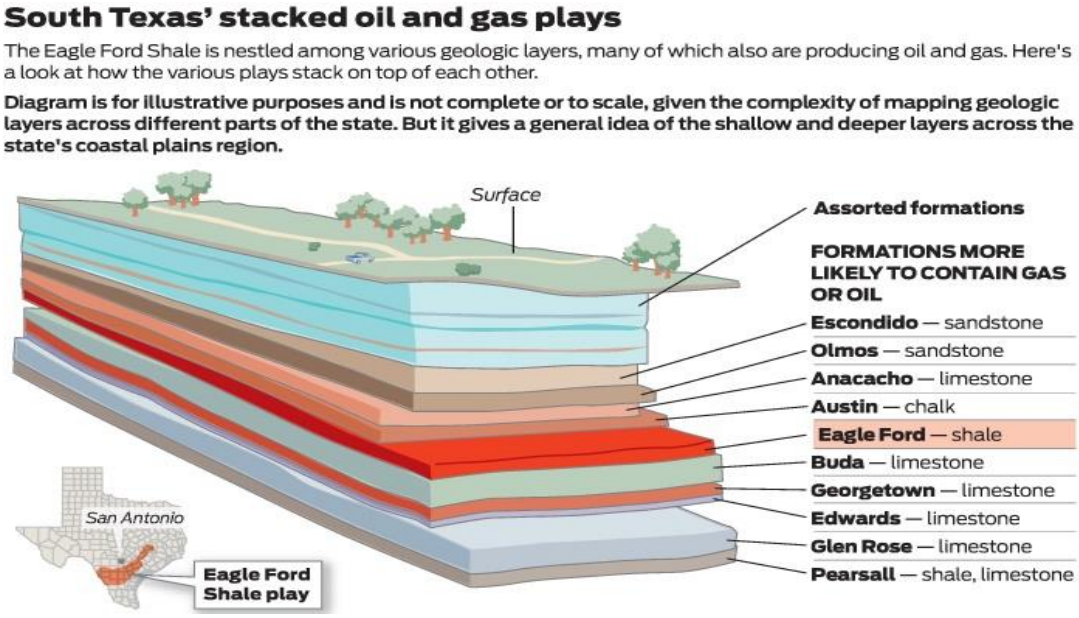

Figure 2.1 Illustrated cross section of subsurface South Texas with EFS.

Modified from University of Texas Bureau of Economic Geology 2016.

2.2 Previous Work

2.2.1 Regional Stratigraphy

The EFS is divided into two primary units the Upper and Lower Eagle EFS. The Upper EFS, which exists solely south of the San Marcos Arch, consists of interbedded low- and high-gamma-ray, burrowed and calcareous mudrock. In contrast, the more organic-rich, Lower EFS, characterized by generally high gamma-ray values, extends continuously from South Texas across to the northeast flank of the San Marcos Arch (Hammes et al., 2016).

Only the Lower EFS crops out southwest of the East Texas Basin and northeast of the Maverick Basin. The Eagle Ford interval, thickest in the Maverick Basin, gradually thins to a minimum over the arch. It continues from the northeast flank of the arch into the southwest East Texas Basin, where the sandstone-rich Woodbine Group occurs between the EFS and Maness Shale (Hentz 2010). The EFS has the facies pinch-out of the Woodbine complex in the northeast and its equivalent Pepper Shale on the basin's southwest flank. Depths of the southeast-dipping Lower EFS range considerably from outcrop to ~17,000ft at the Stuart City shelf margin on the northeast flank of the San Marcos Arch (Hentz and Ruppel, 2010). Regional depth gradients of the unit are greatest on the flanks and crest of the San Marcos Arch (Hammes et al., 2016).

A comprehensive regional stratigraphic column from previous studies was compiled by Melinda Quest (2012) and provides a clearer visual understanding of the Eagle Ford in the subsurface vertical profile of Texas coupled with the eustatic sea level rise and fall (Figure 2.1). The localized south Texas study area is highlighted in red in Figure 2.1.

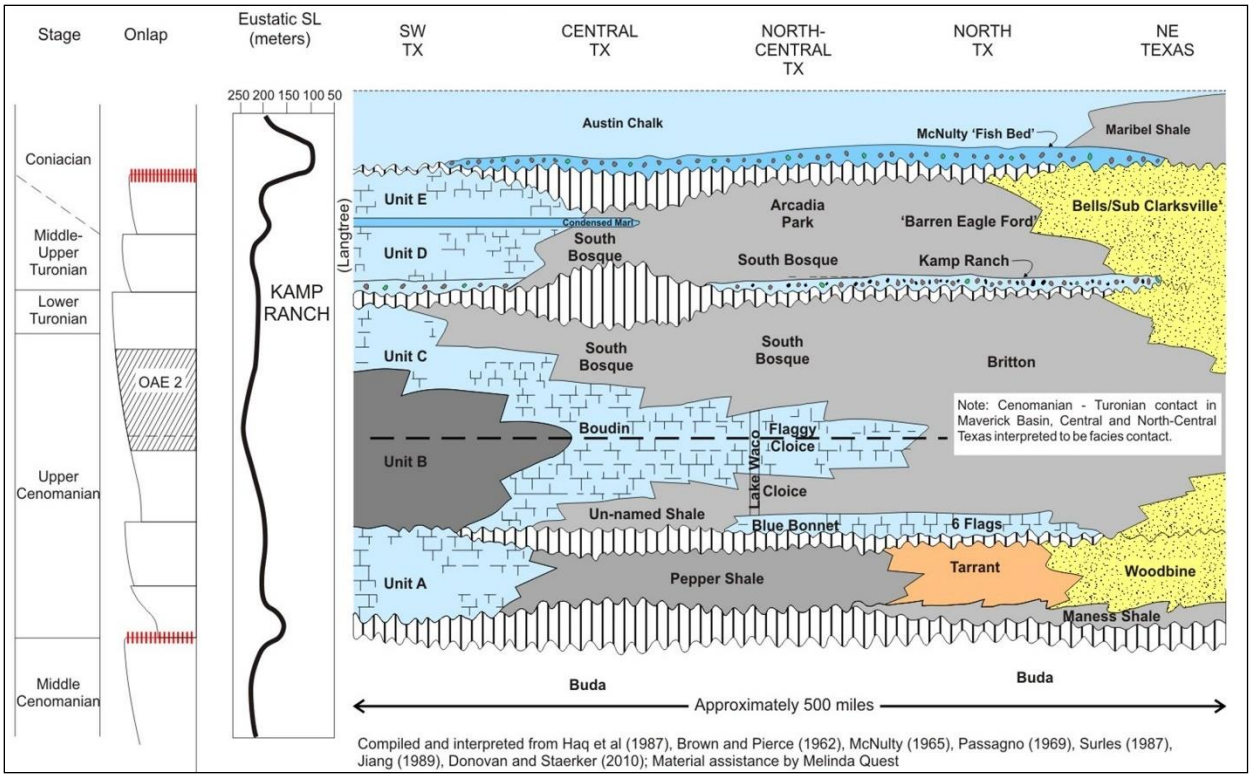

Figure 2.2 Regional stratigraphic column of Eagle Ford Formation and its Cretaceous time equivalents in Texas. South Texas study location in boxed in red.

Modified from Melinda Quest (2012)

The EFS is predominantly composed of organic carbon-rich, fossiliferous, marine shales and marls with interbedded thin limestone beds deposited during a second order transgression on a carbonate-dominated shelf updip from the older Siglo and Edwards reef margin (Harbor, 2011; Hammes 2016). This second order transgressive sea level change was associated with the deposition of the economically produced, organic-rich EFS marls and limestones on the Comanche Platform located south of the Llano uplift, west of the San Marcos Arch and north of the Siglo Reef Margin in South Texas (Figure 2.1) (Phelps et al., 2015).

2.2.2 Tectonic Setting

The Cretaceous Western Interior Seaway (KWIS), also called the Cretaceous Seaway, the Niobraran Sea, and the North American Inland Sea, was created as the Farallon tectonic plate subducted under the North American Plate during the early-Cretaceous (Slingerland et al., 1996). As plate convergence proceeded, the younger and more buoyant lithosphere of the Farallon Plate subducted at a shallow angle (less than 30° to horizontal), in what is known as a "flat slab"(Mitrovica, 1989). This shallowly subducting slab exerted traction on the base of the lithosphere, pulling it down and producing thrust loading flexure subsidence, slab related dynamic subsidence that caused the opening and flooding of the KWIS (Figure 2.2).

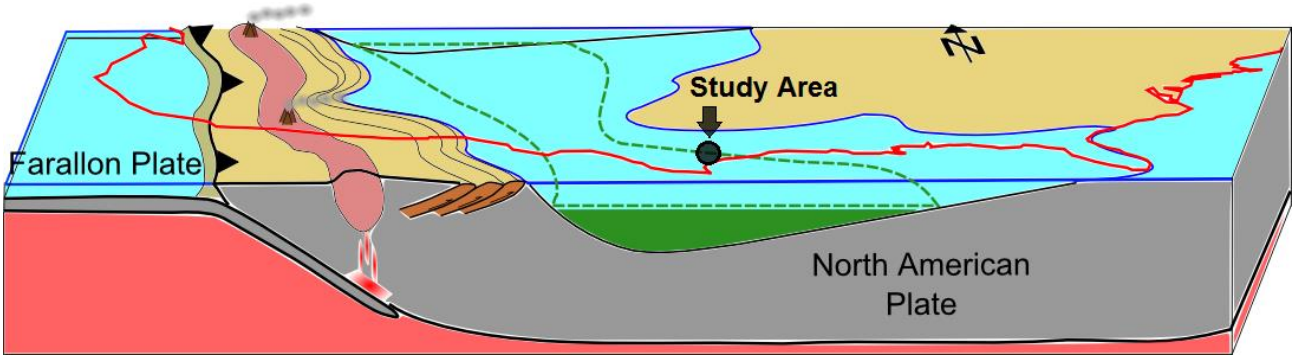

Figure 2.3 An illustration of the Western Interior Seaway during OAEII. The structure of the North American plate and sea level (blue line) projected over the United States of America (red line) with nutrient sourcing from volcanoes along the convergent margin, and the resulting water column stratification (green) and its extent throughout the basin (dashed green line).

Modified from Gross (2012).

The subduction of the oceanic Farallon plate underneath the North American plate is associated with volcanic and plutonic activity and is defined by a western compressional event that transmitted eastward directed thrusts which sheared continental shelf and slope strata exposing the underlying Precambrian basement craton

(Rocky Mountains) (Humphreys et al., 2003). This produced a zone of eastward direction thrust faults and folds that represent 40 to 65 km of crustal shortening in response to compressional forces, Sevier Orogeny.

The regional tectonic setting of the Farallon plate subduction in the west and the resulting Sevier orogeny influenced coupled with high eustatic sea levels existing during the Late Cretaceous, allowed saline waters from the Arctic Ocean in the north and the Gulf of Mexico in the south to meet and flood the central lowlands, forming a sea that transgressed and regressed over the course of the Cretaceous(Haq 2014; Kominz et al. 2008; Muller et al. 2008; Ruban, 2014).

Concurrently in the Late Cretaceous, the Gulf Coast Basin subsided and created accommodation space for mixed siliclastic and carbonate sediments to be deposited during the deposition of organic rich sediment. This accommodation was due to the faults trending southwest-northeast of the remnant Sligo and Edwards-Stuart City reef margins (Scott, 2010; Harbor 2011). The coeval regional tectonic events coupled with episodic volcanic activity may have played a major role in the complex open water-mass exchange between global oceans(Boreal and Tethyan) and the KWIS during peak transgression by increasing delivery of nutrients, enhancing primary production and possibly contributing to the sequestration and preservation of ^{12}C-enriched organic shales like the EFS.

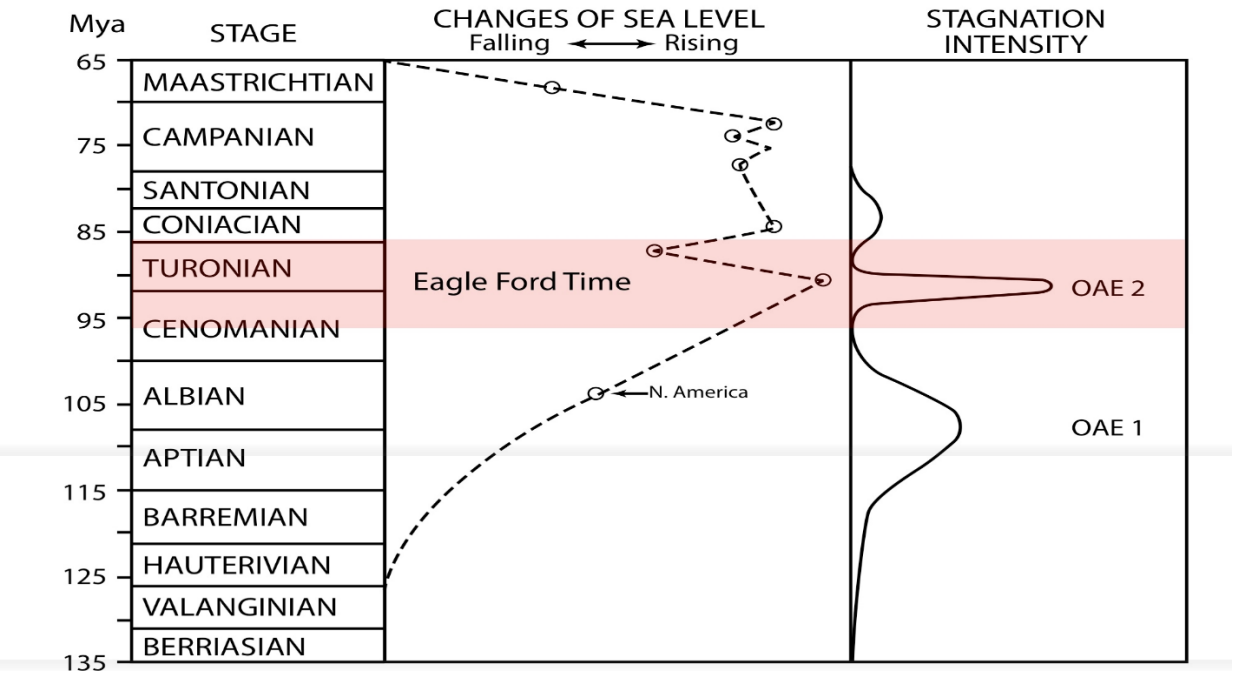

Figure 2.4 Global sea-level second-order sea level curve and water stagnation intensity curve

Modified from Arthur and Schlanger (1979).

The Eagle Ford in South Texas varies in depth from outcrops in the north and northwest to more than 16,000 ft. in the south and southeast as delineated by the structural top of the Buda, a continuous unit underlying the EFS throughout most the formation (Hammes et al., 2016).). The regional tectonic feature which directly influences the deposition and preservation south Texas study area of the EFS include the San Marcos Arch. This paleo-topographic high, has been interpreted to be an extension of the Mesoproterozoic Llano Uplift (Ewing, 2001; Hentz and Ruppel, 2010).

In west Texas, near the Maverick Basin, a northwesterly structural grain with compressional folds and faults is dominant, because of Laramide related deformation caused by uplift of the Sierra Madre Oriental (Goldhammer and Johnson, 2001). In the selected study area located southwest of the San Marcos Arch, a northeast-striking

extensional regime is seen in normal faults and deeper seated, down to- the-basin listric faults (Ewing, 2010). These faults are suggested to have influenced production due to enhancement of fractures in the Cretaceous reservoirs (Tinnin et al., 2014).

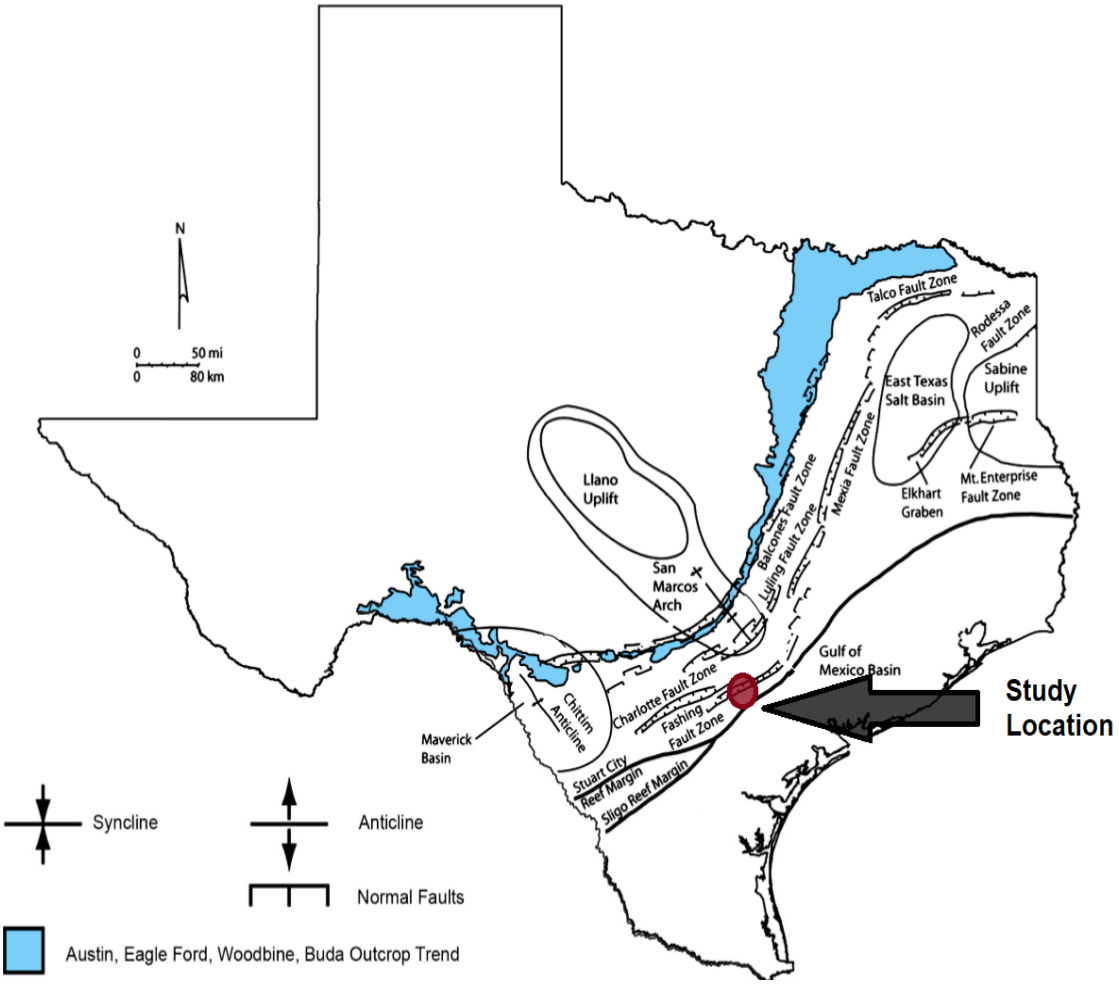

Figure 2.5 Generalized structural features near Late Cretaceous strata in Texas Outcrops are outlined in dark green with study area in circled in red. Modified from Workman (2013).

Major faulting initiated during the Late Jurassic to Early Cretaceous and remained active into the Cenozoic (Harbor, 2011). The Miocene aged Balcones Fault Zone (~25 to 10 Ma) affected the shape of the basin post-OAEII. Studies have shown that all the fault

systems except the Balcones, were active during EFS deposition and affected sedimentation and the eventual outline of the Eagle Ford Formation (Darnaeon, 2013 and references therein). This resulted in landward-dipping grabens between the Luling and Balcones Fault Zones; the faults have shown to trendbasinward and landward-dipping normal faults with graben development in between the Charlotte Fault System and Fashing Fault Zone/Karnes Trough (Harbor, 2011).

2.2.3 Paleogeographic and Paleoclimate Setting

Throughout the Cretaceous, from the late Albian stage to the end of the Maastrichtian, North America was covered with shallow epicontinental marine waters known as the i.e., (KWIS). These shallow seas stretched from Arctic Canada, in the North, to the Gulf of Mexico, in the South, during the maximum flooding extent (Kauffman, 1984). To the east, the KWIS was bordered by the stable North American craton and in the west by a Cordilleran thrust belt with localized volcanic centers in Idaho-Montana and New Mexico-Arizona" (Kauffman, 1977). To the south, the North American shoreline, also known as the "proto-Gulf of Mexico," contained a broad, stable shelf complex, which was subjected to repeated deposition and erosion throughout the Cretaceous (Figure2.5) (Murray et al., 1985; Scott, 2010).

The KWIS recorded five major transgressive-regressive cycles throughout its history (Kauffman, 1984). However, the Upper Cretaceous section of Texas is only divided into three long-term depositional cycles: the Coahuila Series, the Comanchean Series and the Gulfian Series (Surles, 1987). All formations above the Buda Limestone, including the Eagle Ford Formation, are considered part of the Gulfian Series (Scott, 2010). The KWIS was subjected to extensive marine flooding and at times of sea level high stand, it connected the Tethyan and the Boreal seas which (Kauffman, 1977).

The occurrence of Cretaceous-age organic rich mudrocks in the KWIS has shown to correlate with the globally correlated Oceanic Anoxic Events (OAEs) and global sea level changes (Gale et al, 2008). Thick black shales with little bioturbation and characteristic fine laminations have been likeded to global perturbations in marine water chemistry, increased atmospheric CO_2, increased volcanic activity, sluggish circulation and large-scale marine transgressions (Schlanger and Jenkyns, 1976; Arthur and Sageman, 1994; Algeo et al., 2008). The decreased oxygen content of Cretaceous marine waters at the time of the OAEs provided some of the mechanisms for massive deposits of the EFS. The (C/T) transition marked by the OAEII and consistently records significant positive excursions of $\delta^{13}C_{org}$ due to the increased burial of ^{12}C organic carbon material (Arthur and Schlanger, 1979; Arthur et al., 1988). Although we know that OAEs are short lived episodes (< 1Ma) of widespread marine anoxia during which large amounts of organic carbon were buried on the ocean floor under oxygen-deficient bottom waters, the exact trigger for the increased preservation of organic matter into the sedimentary record is still in question.

The EFS was deposited during a time of increased bio productivity on a global scale (e.g., Tethys Sea, Atlantic and Equatorial Pacific) coeval with the OAE II (Kuroda et al., 2007). Most subsurface and outcrop studies of the KWIS suggest the OAEII initiated before the Cenomanian-Turonian boundary, which has been placed at 93.9 Ma by Walker et al., 2012. OAEs are geological time intervals characterized by extremely high burial rates of organic- carbon that resulted in global formation of black, organic-rich shales (Kuroda et al., 2007; Turgeon and Creaser, 2008). OAEs represents a period of sluggish ocean circulation and may be caused by a voluminous release of methane from gas hydrates in marine sediments, massive volcanic events or water displacement caused

from sea-floor spreading at mid-ocean ridges (Kuroda et al., 2007; Mort et al., 2010; Hetzel et al., 2011).

2.2.4 Volcanism and Igneous Provinces

The Late Cretaceous deposition of the EFS was accompanied by extended periods of volcanism; both submarine volcanism in large igneous provinces(LIPs) and island arc volcanism from the Sierran and Carribean arc (Figure 2.5) (Turgeon and Creaser, 2008; Adams and Carr, 2010; Blakey 2013). Global studies have suggested that the emplacement of LIP's, mid ocean ridges or crustal volcanism contributed to the initiation of OAEII by releasing large quantities of CO_2 which accumulated in the atmosphere and sea surfaces. The surplus of CO_2 in the atmosphere maximized global greenhouse effects, increased surface ocean temperatures, and contributed to the decline of primary producers (phytoplankton) due to acidification (Turgeon and Creaser 2008).

Previous investigations have shown geochemical evidence for the occurrence of massive volcanic eruptions associated with the emplacement of LIPs as a trigger for globally distributed black shale deposition (Kuroda et al., 2007, Derek et al., 2010). In the KWIS, pyroclastic debris were first described as bentonite bed in sub surface cores (Hunter and Davies, 1979). Intermittent bentonite beds have been identified throughout Upper and Lower Eagle Ford outcrops and subsurface cores, suggesting volcanism was continuous throughout the time of deposition. Although contemporaneous volcanism was prominent throughout the Late Cretaceous, identifying the localized source for the bentonite beds of the south Texas EFS is still challenging due to the complex heterogenic nature of the formation.

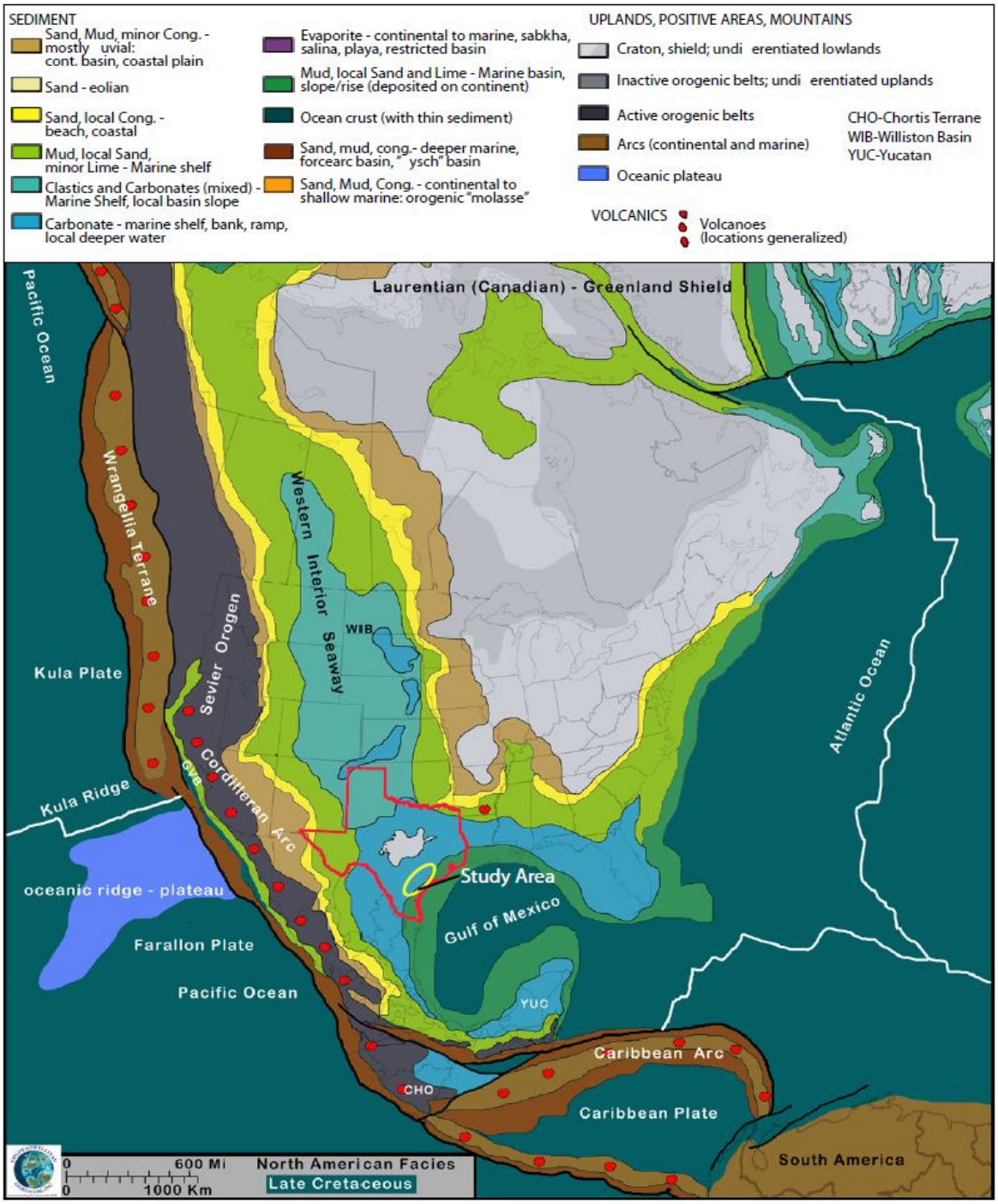

Figure 2.6 Late Cretaceous paleotectonism and sedimentation in proximity of study area

Modified from Blakey (2013).

2.2.3.1 Geochemical Proxies

Geochemical proxies have proven useful in to reconstruct paleoenvironmental conditions that control the formation, deposition and preservation of organic rich sediments like the (C/T) EFS of South Texas.

Paleo productivity is a measurement of past production levels within the Earth's various ecosystems. It is usually measured using the deposits or chemical remnants of production, which have been locked into the Earth's sediments. Although several well-established geochemical proxies exist for paleo productivity, few published data sets exist which focus directly on the EFS.

Kearns (2011) completed a multi-proxy study on cores from the EFS and he cited the usefulness of elemental proxies established by (Tribovillard et al., 2006; Brumsack 2006) identifying trace metals (Mo, V, Ni. Cu and U) as redox properties. (Tribovillard et al., 2006) provided a fundamental synthesis of the use of trace elements as proxies and confirmed that redox-sensitive trace metals tend to be more soluble under oxidizing conditions and less soluble under reducing conditions, resulting in authigenic enrichments in oxygen-depleted sedimentary facies. This inherent solubility mechanism makes U, V and Mo, and to a lesser extent certain other trace metals such as Cr and Co, useful as paleo redox proxies. Phosphorous is also used as a paleoproductivity proxy because it is a limiting macronutrient for algal growth (Calvert and Pedersen, 2007), but it has been correlated to suggest pulses of increased upwelling throughout the deposition of the Eagle Ford (Tinnin et al., 2013). In some cases, some redox sensitive elements (Ni, Cu, Zn) are mostly deposited as organometallic complexes. During organic matter decay, these elements may be incorporated into pyrite under sulfate reducing conditions (Brumsack, 2006; Tribovillard et al., 2006).

Several redox-sensitive elements are delivered to the sediment mainly in association with organic matter (Ni, Cu, Zn, Cd) and they may be retained within the sediment in association with pyrite, after organic matter decay in reducing sediment. Particularly Ni and Cu are good values as proxies for organic C sinking flux (frequently referred to as productivity)(Zhao et al., 2016).

The oxyanions Mo, U and V show different behaviour under various redox conditions (Tribovillard et al., 2006). While U and V may be reduced and accumulated under denitrifying (suboxic-anoxic) conditions, Mo is enriched mainly under sulfate-reducing (anoxic-sulfidic) conditions. Thus, in the case of U and V enrichment without parallel Mo enrichment, suboxic/anoxic depositional conditions without free hydrogen sulphide are suggested (Tribovillard 2006).

Although U and Mo have been used to examine redox conditions and processes in marine sediments by using Enrichment Factors (EF) to identify three patterns of U–Mo covariation (unrestricted marine systems, strongly restricted basin and weakly restricted basin), each of which is related to a different modern marine setting (Algeo and Tribovillard 2009).

Enrichment Factors can help show correlations in the degree of enrichment or depletion relative to the average post-Archean shale (PAAS) concentrations. PAAS concentrations from Taylor and McLennan (1985) are implemented to show the degree of enrichment or depletion of an element within the Eagle Ford. By incorporating the EF relative to PAAS, we can better interpret the volcanogenic elemental enrichment relative to the average continental crust.

Chapter 3

METHODLOGY

3.1 Study Design

A localized core from south Texas was studied by analyzing whole rock samples. The core represents a continuous 300ft interval at approximately ~13,000ft below the surface. To better characterize and interpret the subsurface core, a multi-faceted approach was implemented to obtain reliable geochemical data. Preliminary major, minor and trace elemental analysis was conducted and the results were incorporated into Darmaoen (2013). This initial data set provided a framework to choose volcanically enriched horizons to perform further higher resolution analysis using Energy Dispersive X-ray Fluorescence (ED-XRF)

3.2 Inductively Coupled Plasma-Mass Spectrometry (ICP-MS)

A data set was compiled with a total of 40 drill cutting samples through Inductively Coupled Plasma-Mass Spectrometry (ICP-MS) analysis by Chemostrat Inc in in Houston Texas in 2013. Major, minor and trace elemental analysis was conducted from a depth of 13122 to 13415 ft. at a 10-15 ft. interval

3.3 Energy Dispersive X-Ray Fluorescence (ED-XRF)

Using previous collected data sets, a highly enriched trace metal interval (13165-13235') concurring with OAE-2, was selected to run high spatial resolution analysis at 1ft intervals. The Shimadzu EDX-7000 spectrometer in the Center for Environmental Forensics and Material Science was used to measure trace metal concentration in each sample. The chamber was purged with helium before each run to minimize interference

from atmospheric signals and help ensure accuracy for highly sensitive light elements. The EDX-700 is outfitted with a high-performance SDD-EDS detector and optimized hardware to achieve a high level of stability, sensitivity, analysis speed, and energy resolution. The core samples were analyzed on the clean and dried side of the core. Samples that were not suitably flat were taken slightly above or below the 1ft interval.

Figure 3.1 Shimadzu EDX-7000

The EDX-7000 can analyze samples individually on a platform using a rotary table.

Two phases of data acquisition were undertaken on each marked stratum. The inorganic elemental suite was generated using two separate and distinct data acquisitions for each sample. Major element data acquisition, including V and Cr measurements, was undertaken using a low-energy, helium purge instrument setting. Trace element data acquisition was undertaken using a filtered, high-energy instrument setting. Both low and high energy analyses were undertaken at the same location on the core face. Major lithoclasts were avoided to minimize unrepresentative measurements.

Low-energy spectrum acquisition includes elements that emit characteristic x-rays between 1.25 to 7.06 kV. In order to obtain the elements in this range, and allow for backscatter that does not interfere with the peaks of interest, the voltage on the instrument was set to 15 kV and the instrument current was set to 42 μA. The characteristic x-rays between 6.92 and 19.80 kV were measured in the high-energy acquisition mode (40 kV and 28 μA). While a filter was used to prevent the low-energy x-rays from reaching the detector, a vacuum pump was not necessary because the energies of x-rays emitted from heavier elements are not attenuated in the short distance between the sample and the detector. The filter consists of 0.006” Cu, 0.001” Ti, and 0.012” Al and is selected respectively to the x-ray energy characteristic of the element being measured directly into the instrument. High-energy acquisitions were taken for 5 minutes and the low-energy acquisitions were for 3 minutes.

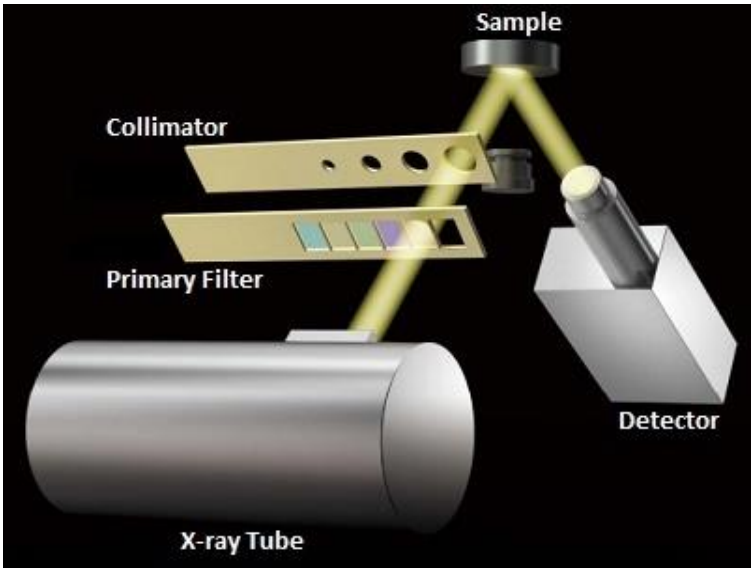

Figure 3.2 Shimadzu EDX-7000 analysis process

The EDX-7000 switches filters depending on the energy range of the element analyzed.

Modified from Shimadzu Corportation 2017

3.3.1 EDX-700 Mudrock Calibration

The raw spectra obtained during the analysis are acquisition are qualitative and require a calibration to convert the data into quantitative weight percentages. The calibration for the EDX-7000 unit is matrix-specific, so a calibration for major and trace elements of mudrocks was developed using a suite of 3 reference materials (SDO-1, SBC-1, SGR-1) that were accurately weighed and mixed to specific proportions (50/50) to produce 6 standards for calibration provide a table of these values and proportions. The low energy calibration quantifies the following elements: Mg, Al, Si, P, S, K, Ca, Ba, Ti, V, Cr, Mn, and Fe. The high energy calibration quantifies the following elements: Ni, Cu, Zn, and Mo.

3.3 U-Pb Geochronology of Ash Bed Zircons

Multiple thin intermittent bentonite beds appear throughout the 300ft subsurface core. Two bentonite beds were sampled for analysis U-Pb. One at the contact between the top of the Eagle Ford and the Austin Chalk, and a second bentonite bed located near the inferred (C/T) boundary was also sampled to help geochronologically constrain and correlate the elemental and isotopic values within the core. The beds were sampled and crushed with agate mortar and pestle, then sieved using stainless steel wire cloth No. 200 (75µm) to separate the smaller ash deposited zircons. This finer fraction was then refined through heavy liquid separation using Bromoform with density 2.89 g/cm3.

After two days the denser zircon (4.85 gm/cc) and apatite (3.18 g/cm3) rich fraction had settled out and samples were left to dry. Due to the similar petrographic characteristics between apatite and zircon, mineral identification was determined through microscopy by immersing grains in methylene iodide with known refractive index value of 1.74. Apatite has an RI value of (1.634–1.638) and zircon of (1.93 – 1.987) respectively. Therefore, when immersed in the liquid, apatite showed no visible relief and zircon were more easily identified and sampled. U-Pb geochronology of zircons was conducted by laser-ablation–multicollector inductively coupled plasma–mass spectrometry at the University of Arizona Laser Chron Center. Details of the method are described in Gehrels et al. (2006).

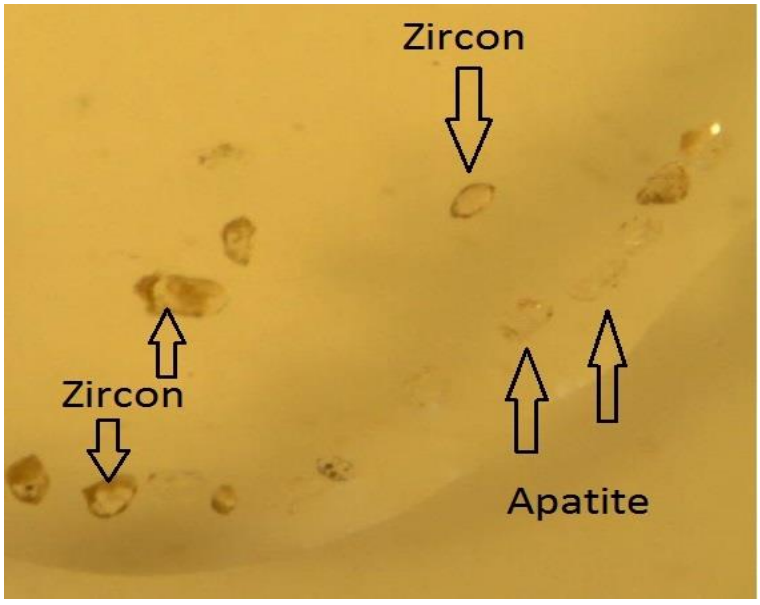

Figure 3.3 Zircon high relief identification relative to apatite

Refractive Index Separation in petrographic microscope

3.4 Non-XRF Geochemical Data

Stable carbon and oxygen isotopes ($\delta^{13}C_{inorg}$ and $\delta^{18}O$), were analyzed by T. Quinn at the Department of Earth and Environmental Science at the University of Texas at Austin. The core was sampled at a 10-15ft resolution and stable isotope were analyzed using a Thermo Electron Kiel IV automated carbonate device connected to a Thermo Electron MAT253 or Delta V dual inlet isotope ratio mass spectrometer (IRMS). Total Organic Carbon (TOC) was measured using the Shimadzu TOC-V_{WS} in conjunction with the solid sample module SSM-500A in the Center for Environmental Forensic and Material Science. The Light Stable Isotope Laboratory at the University of Texas at Arlington provided the organic stable carbon isotope $\delta^{13}C_{org}$ analysis. A Finnegan Delta V Advantage isotope ratio mass spectrometer, a Gasbench II, and an Elemental Analyzer were used to process the samples and retrieve $\delta^{13}C_{org}$ values.

3.4.1 Stable Isotope $\delta^{13}C_{inorg}$ and $\delta^{18}O$

Stable isotopic compositions of $\delta^{13}C_{inorg}$ and $\delta^{18}O$ were performed on powdered samples that were weighed into silver capsules (Costech Analytical, Inc. #41067) and subsequently acidified repeatedly with 6% sulfurous acid (H2SO3) to remove carbonate phases (Verardo et al., 1990). Stable isotope determinations were made on aliquots of sample powder using a Thermo Electron Kiel IV automated carbonate device connected to a Thermo Electron MAT253 or Delta V dual inlet isotope ratio mass spectrometer (IRMS), both at the Analytical Laboratory for Paleoclimate Studies (ALPS) at the Jackson School of Geosciences, University of Texas at Austin. The long-term precision of the Kiel IV/MAT253/Delta V IRMS is 0.08‰ for δ18O and 0.04‰ for $\delta13C_{inorg}$ (1σ), as estimated via multiple analyses of carbonate standards of known isotopic composition (NBS-19,

Estremoz). All stable isotope values are reported relative to Vienna Pee Dee Belemnite (VPDB), in standard delta notation.

3.4.2 Total Organic Carbon (TOC)

Core samples were taken at intervals of 10ft and ground to a fine powder using a Spex Mill/Mixer. A 20-40mg aliquot of the sample was first analyzed for Total Carbon (TC). Subsequently, another 15-30mg of the sample was analyzed for Inorganic Carbon (IC). After the two values for the sample are determined, TOC can be obtained by subtracting the IC from the TC. Precision of these values are ensured by running two USGS shale samples (SGR-1 and SDO-1) at the beginning and the end of each run along with a standard check every five samples.

3.4.3 Stable Isotope $\delta^{13}C_{org}$

Samples were analyzed at the University of Texas at Arlington using a Costech ECS 4010 elemental analyzer interfaced with a Thermo Finnigan Conflo IV device to a Thermo Finnigan Delta-V isotope-ratio mass spectrometer (IRMS). Isotopic results are reported in per mil (‰) relative to V-PDB for δ 13C. The average standard deviations were 0.13‰ and 0.08‰ for δ 13C of USGS-40 glutamic acid (IAEA-8573). and 0.39% and 0.01% for the TOC and TN of USGS-40, respectively.

Chapter 4

RESULTS

4.1 Geochemical Analysis

The comprehensive ICP-MS major, minor and trace elemental analyses collected by Chemostrat Inc., provided precise and accurate results which clearly demonstrated the geochemical variability throughout the 300ft core. This initial, laboratory-derived, data set provided a clear framework to select horizons shown to be enriched with volcanogenic elements. These horizons were specifically selected to perform further higher resolution analysis using the EDX-7000. The laboratory-derived data was used to confirm the results of the EDX-7000 data set since the ICP-MS with fusion fluxes for preparation of samples have less uncertainty. The EDX-7000 data set is not as comprehensive as the ICPMS data set, but is rather restricted to a smaller interval at a higher resolution to demonstrate the geochemical heterogeneity and volcanogenic enrichment in the core at higher resolution (i.e. 1 ft. interval).

These geochemical data sets were geochronologically constrained by the sampled bentonite bed zircons near the inferred C/T boundary and the global $\delta^{13}C_{org}$ excursion which helps constrain the extent of OAEII in this localized subsurface core. The tops and bottoms of the formations were confirmed through supplementary gamma ray logs provided by Core Laboratories..

4.1.1 Inductively Coupled Plasma-Mass Spectrometry (ICP-MS)

4.1.1.1 Major and Minor Elemental Results

A total of 40 drill cutting samples were analyzed through Inductively Coupled Plasma-Mass Spectrometry (ICP-MS) analysis. Major elemental analysis show the lithological heterogeneities and oscillations from a more calcium rich mud stone to a more clay and silica rich mud stone (Figure 4.1) .

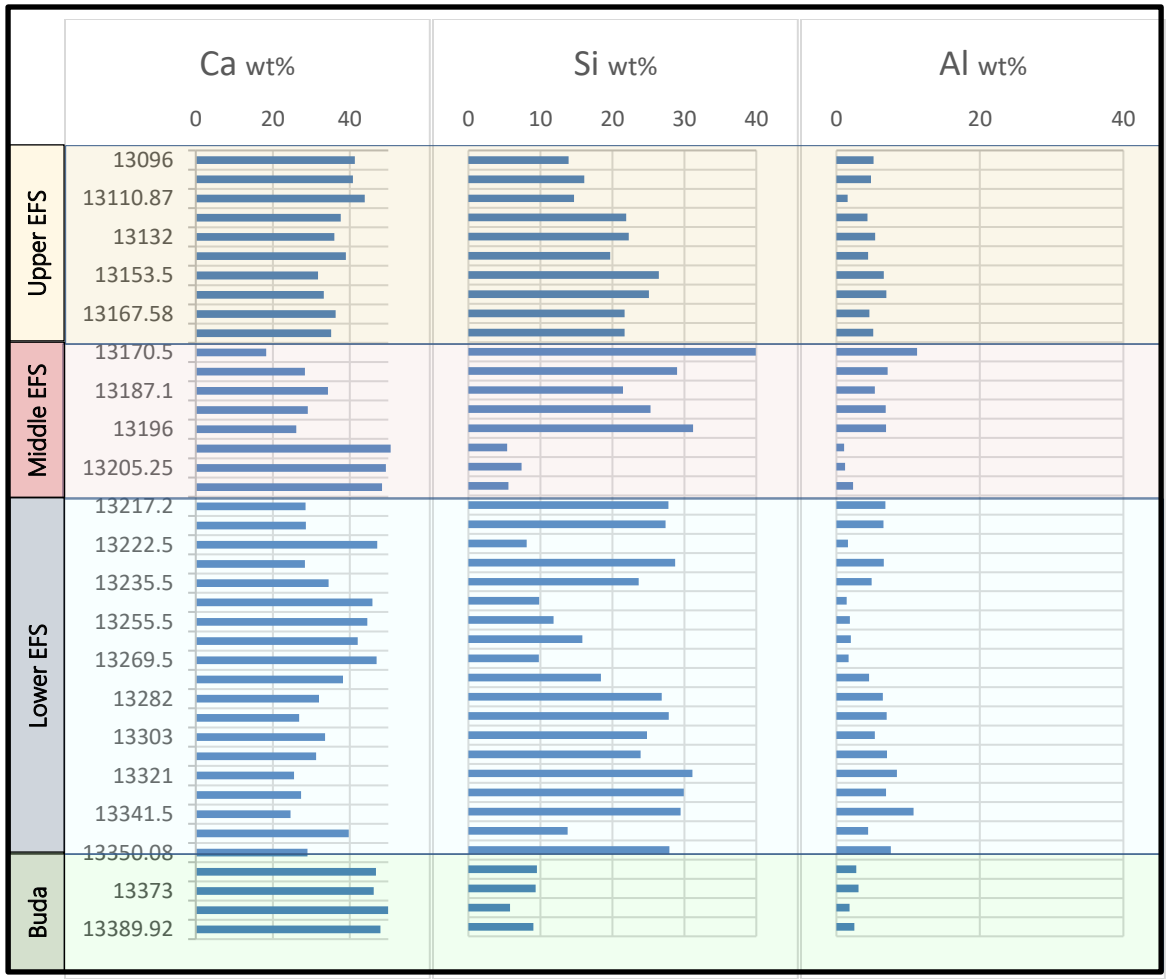

Figure 4.1 Subsurface EFS core major element (Ca, Si, and Al) concentrations in weight %

Starting at the base of the subsurface core vertical profile (Figure 4.1), major element results show a sharp transition from the primarily, calcium carbonate, Buda Limestone to the more silca and aluminum rich Lower Eagle Ford. Going up section the Lower Eagle grades from a less calcium rich and more silica and aluminum rich facies to a higher calcium and lower aluminum rich facies at the top of the unit. The Middle Eagle Ford contains reaches highest concentrations of aluminum and silica generally decreases in calcium going up section. The Upper Eagle Ford is consistently more enriched in calcium carbonate and silica with low aluminum relative to the rest of the units.

4.1.1.2 Minor and Trace Elemental Results

The whole rock, subsurface black shale samples shows elevated concentrations of volcanogenic trace elements (Co, Cr, Cu, Ni, Mo and Zn) throughout the core. Highly enriched intervals are highlighted in red showing the maxim elemental values throughout the core (Figure 4.2). Elemental values (Co, Cr, Cu, Ni, Mo and Zn) shown in Figures (4.3) and (4.4) present the values in the form of a bar graph with maximum, minimum and percent change calculated for each element.

Three highly enriched intervals were identified throughout the EFS the core and showed an ~80-99% increase in abundance of Co, Cr, Cu, Ni, Mo and Zn. Peak concentrations were given in parts per million(ppm) and reached values of 15, 144, 82, 100, 213 and 317 for Co, Cr, Cu, Ni, Mo and Zn respectively. A significant depletion was noted after the second enriched horizon for a 10 ft. interval from 13200 – 13210 ft. Minimum concentrations were reached ppm values of 2.3, 14.7, 4, 5, 9 and 14 for Co, Cr, Cu, Ni, Mo and Zn respectively. The third enriched horizon occurs in the Middle EFS and is located directly above the concentration minimums seen in the core.

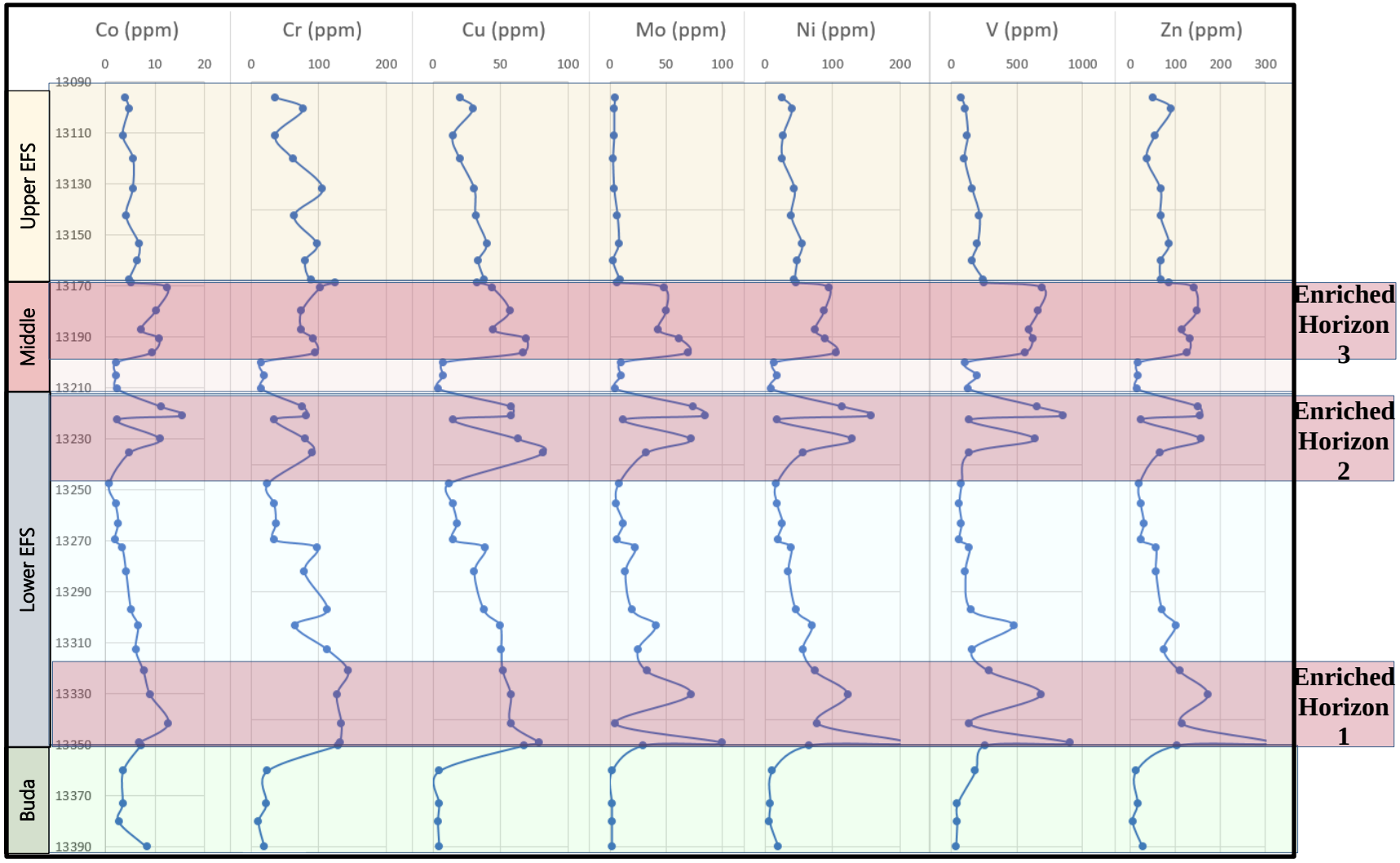

Figure 4.2 Subsurface EFS core Minor and Trace element (Co, Cr, Cu, Mo, Ni V and Zn) concentrations in ppm

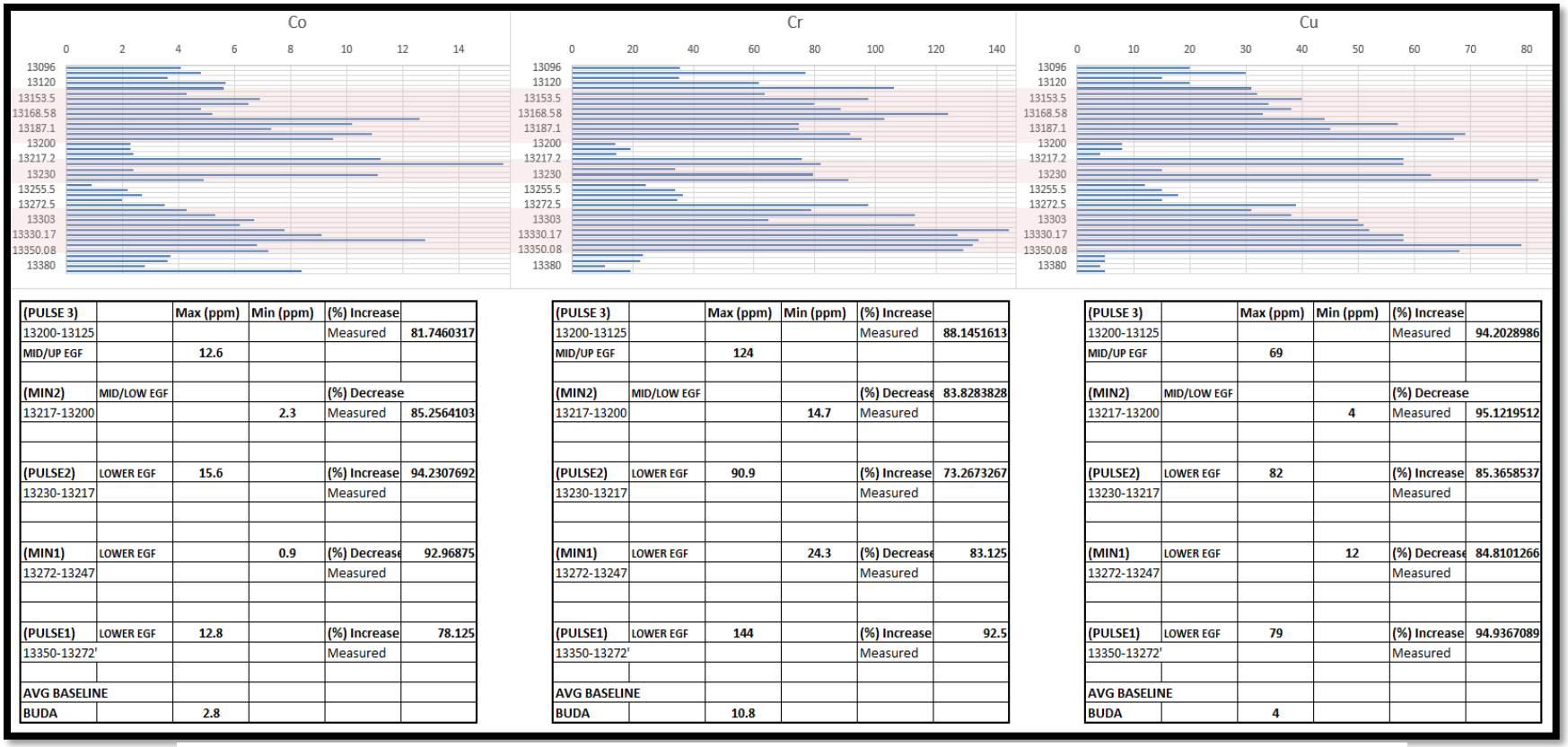

(PULSE 3)		Max (ppm)	Min (ppm)	(%) Increase	
13200-13125				Measured	81.7460317
MID/UP EGF		12.6			
(MIN2)	MID/LOW EGF			(%) Decrease	
13217-13200			2.3	Measured	85.2564103
(PULSE2)	LOWER EGF	15.6		(%) Increase	94.2307692
13230-13217				Measured	
(MIN1)	LOWER EGF		0.9	(%) Decrease	92.96875
13272-13247				Measured	
(PULSE1)	LOWER EGF	12.8		(%) Increase	78.125
13350-13272'				Measured	
AVG BASELINE					
BUDA		2.8			

(PULSE 3)		Max (ppm)	Min (ppm)	(%) Increase	
13200-13125				Measured	88.1451613
MID/UP EGF		124			
(MIN2)	MID/LOW EGF			(%) Decrease	83.8283828
13217-13200			14.7	Measured	
(PULSE2)	LOWER EGF	90.9		(%) Increase	73.2673267
13230-13217				Measured	
(MIN1)	LOWER EGF		24.3	(%) Decrease	83.125
13272-13247				Measured	
(PULSE1)	LOWER EGF	144		(%) Increase	92.5
13350-13272'				Measured	
AVG BASELINE					
BUDA		10.8			

(PULSE 3)		Max (ppm)	Min (ppm)	(%) Increase	
13200-13125				Measured	94.2028986
MID/UP EGF		69			
(MIN2)	MID/LOW EGF			(%) Decrease	
13217-13200			4	Measured	95.1219512
(PULSE2)	LOWER EGF	82		(%) Increase	85.3658537
13230-13217				Measured	
(MIN1)	LOWER EGF		12	(%) Decrease	84.8101266
13272-13247				Measured	
(PULSE1)	LOWER EGF	79		(%) Increase	94.9367089
13350-13272'				Measured	
AVG BASELINE					
BUDA		4			

Figure 4.3 Subsurface EFS core Minor and Trace element (Co, Cr, and Cu) concentrations in ppm. Enriched intervals are highlighted in red and maximum/minimum values are given in the chart

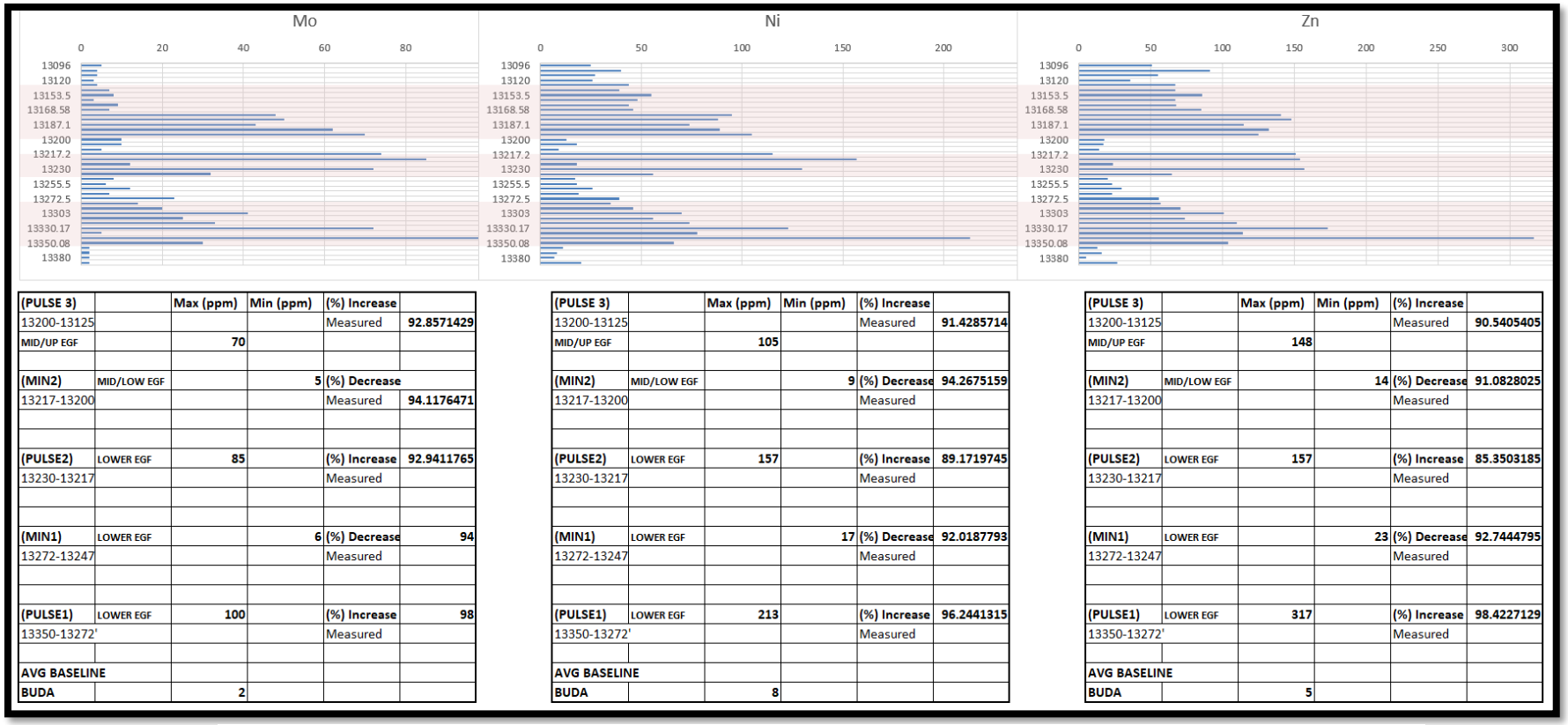

(PULSE 3)		Max (ppm)	Min (ppm)	(%) Increase	
13200-13125				Measured	92.8571429
MID/UP EGF		70			
(MIN2)	MID/LOW EGF		5	(%) Decrease	
13217-13200				Measured	94.1176471
(PULSE2)	LOWER EGF	85		(%) Increase	92.9411765
13230-13217				Measured	
(MIN1)	LOWER EGF		6	(%) Decrease	94
13272-13247				Measured	
(PULSE1)	LOWER EGF	100		(%) Increase	98
13350-13272'				Measured	
AVG BASELINE					
BUDA		2			

(PULSE 3)		Max (ppm)	Min (ppm)	(%) Increase	
13200-13125				Measured	91.4285714
MID/UP EGF		105			
(MIN2)	MID/LOW EGF		9	(%) Decrease	94.2675159
13217-13200				Measured	
(PULSE2)	LOWER EGF	157		(%) Increase	89.1719745
13230-13217				Measured	
(MIN1)	LOWER EGF		17	(%) Decrease	92.0187793
13272-13247				Measured	
(PULSE1)	LOWER EGF	213		(%) Increase	96.2441315
13350-13272'				Measured	
AVG BASELINE					
BUDA		8			

(PULSE 3)		Max (ppm)	Min (ppm)	(%) Increase	
13200-13125				Measured	90.5405405
MID/UP EGF		148			
(MIN2)	MID/LOW EGF		14	(%) Decrease	91.0828025
13217-13200				Measured	
(PULSE2)	LOWER EGF	157		(%) Increase	85.3503185
13230-13217				Measured	
(MIN1)	LOWER EGF		23	(%) Decrease	92.7444795
13272-13247				Measured	
(PULSE1)	LOWER EGF	317		(%) Increase	98.4227129
13350-13272'				Measured	
AVG BASELINE					
BUDA		5			

Figure 4.4 Subsurface EFS core Minor and Trace element (Mo, Ni, and Zn) concentrations in ppm. Enriched intervals are highlighted in red and maximum / minimum values are given in the chart

4.1.2 Single Crystal U-Pb Geochronology of Zircons

By sampling bentonite bed zircons near the inferred C/T boundary, U-Pb age of 93.2 ±1.7 Ma for the Eagle Ford is established. The contact with overlying Austin Chalk can also be constrained at 85.76 ±1.2-0.58Ma from the U-Pb age given from the bentonite bed at the contact. This date falls precisely within the range of the (C/T) boundary extinction the relatively small size of the zircon grains suggest they were light enough to have been carried by volcanic ash and are likely from proximal volcanic source.

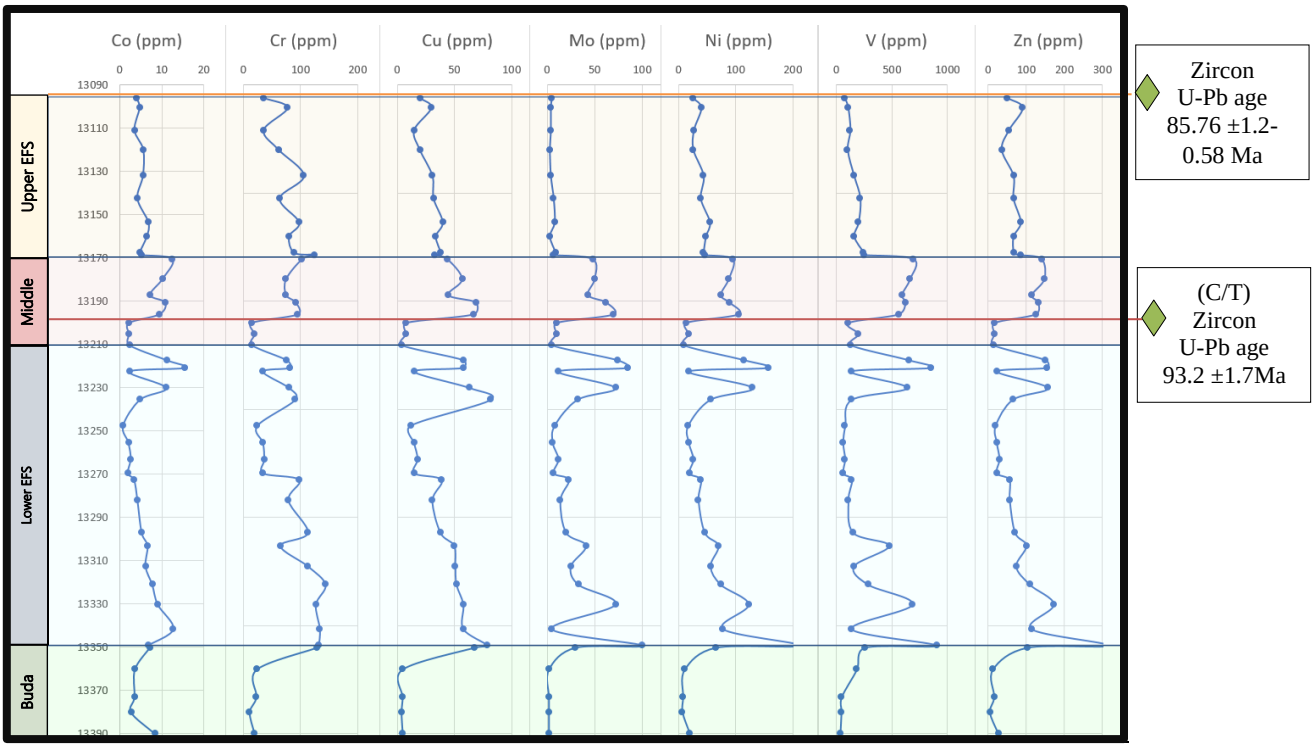

Figure 4.5 U-Pb dated bentonite zircons from Upper and Middle EFS plotted on elemental graphs,

4.1.3 Energy Dispersive X-Ray Fluorescence (ED-XRF)

The highly enriched trace metal interval (13165-13235') concurring with OAE-2, was selected to run high resolution analysis at 1ft intervals. The results are compared to the ICP-MS data collected by Chemostrat and the general increased trends do appear to correlate. However, at higher resolution we see high frequency of oscillations likely reflecting the finely laminated lithologic variations seen at high resolution.

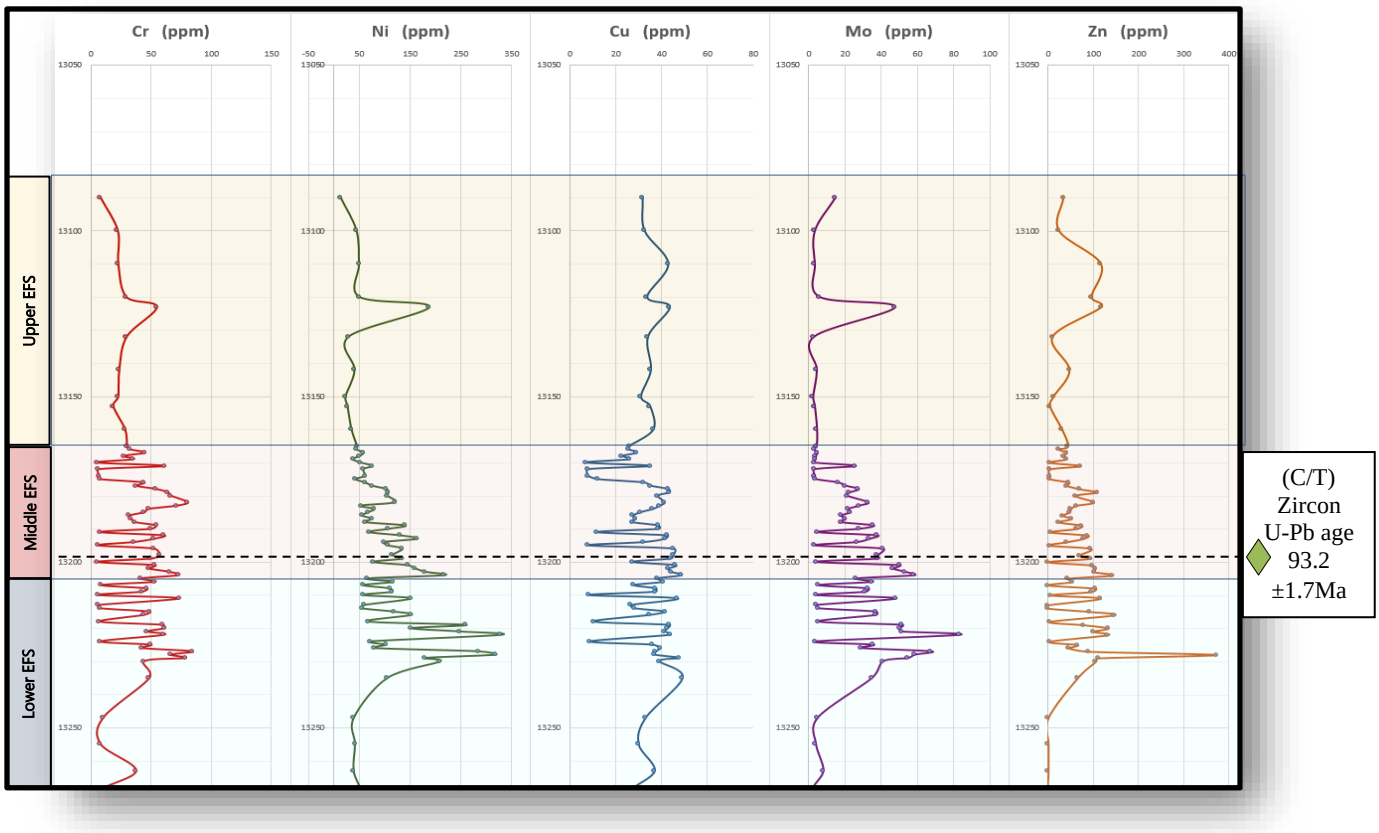

Figure 4.6 Energy Dispersive X-ray Fluorescence minor and trace elemental plots of EFS

4.1.4 $\delta^{13}C_{org}$ $\delta^{13}C_{inorg}$ $\delta^{18}O$ and TOC

The Stable isotopic compositions of $\delta^{13}C_{carb}$ and $\delta^{18}O$ show possible correlation with the geochronologically interpreted C/T boundary with the highest $\delta^{18}O$ value and lowest $\delta^{13}C_{carb}$ value occurring directly after the second(~2%) increase in $\delta^{13}C_{org}$.

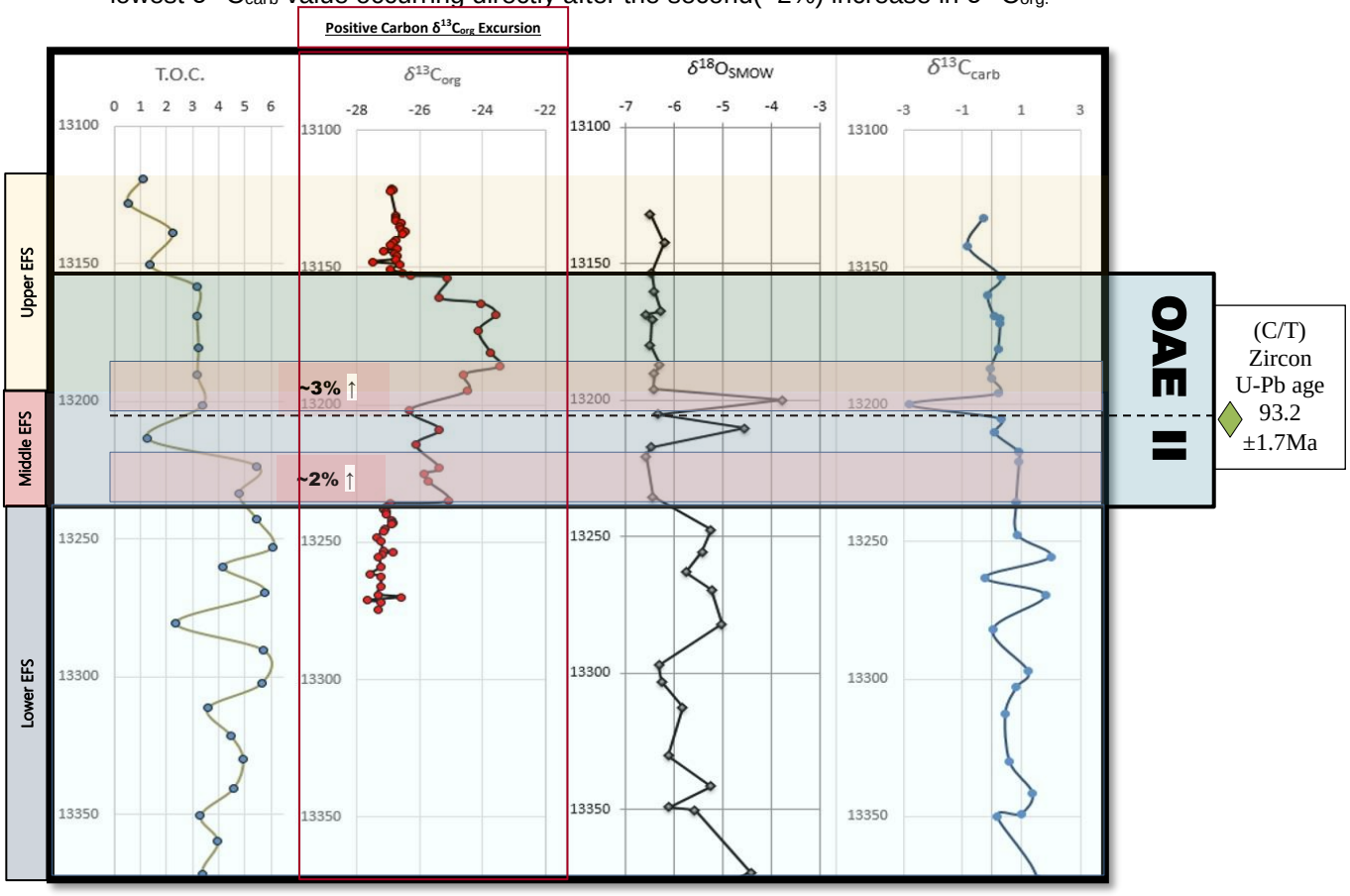

Figure 4.7 Plots of $\delta^{13}C_{org}$, $\delta^{13}C_{inorg}$, $\delta^{18}O$ and TOC of EFS. OAEII and positive carbon isotope excursions are highlighted blue and red respectively.

The globally recognized $\delta 13C_{org}$ positive excursion was established in the localized subsurface EFS core -The onset of the Carbon (δ13C) excursion first appears ~45ft before the dated zircons and shows an initial ~2% increase from -27.05% to -25.09%. At approximately 1ft above the C/T dated bentonite bed we see a secondary

~3% increase from -26.31% to -23.45% over a 10 ft. interval for (δ13C) values correlating with increased volcanic trace metal signatures. OAEII, defined by the positive carbon ($\delta^{13}C$) isotope excursion, was found to span over an interval of ~85 ft. from (13236-13154 ft.).

Chapter 5

DISCUSSION

5.1 Elemental Interpretations

5.1.1 Study Findings

The primary goal of this thesis was to illustrate the geochemical heterogeneity and volcanic enrichment in the EFS subsurface core of South Texas. The vertical depth profiles were created to illustrate the elemental variations, enrichments and correlations seen throughout the EFS. The transition between the Buda, Lower EFS, Middle EFS, and Upper EFS were all confirmed by the gamma ray log provided by Chemostrat Inc. The sharp increases in gamma ray API units are used as transition markers for the lower middle and upper contacts (Figure 5.1)

The U-Pb bentonite age of 93.2 ±1.7Ma near the inferred (C/T) boundary confirmed the $\delta 13C_{org}$ positive excursion used to define the OAEII. The analytical results show significantly increased volcanogenic trace metal input correlating with increased Total Organic Carbon and positive $\delta^{13}C$ values at the C/T dated zircon horizon. However, immediately preceding the C/T transition boundary, but after the onset of OAEII, a drop in volcanogenic trace metal input and TOC is seen. Concurrently, calcium carbonate shows sharp increase while silica and aluminum reach minimum values recorded throughout the core. Using paleo environmental proxies (i.e. C/Al) we can infer a eustatic transgressive sea level rise gave rise to the maximum flooding surface and likely depleted the enriched signal of volcanogenic elements. This data suggests the volcanically enriched horizons likely were continuous throughout the OAEII and eustatic transgressive sequences decreased the ability for the elements to be preserved preceding the C/T transition boundary. The interpretations presented in this section help support the possible volcanogenic enrichment and inferred geologic age of the OAEII and C/T global event.

5.1.2 Major and Minor Element Interpretation

Aluminum is used as a proxy for the clay content of the core. Calcium carbonate shows an inverse trend with aluminum and silica. Marl or marlstone is a calcium carbonate or lime-rich mud or mudstone which contains variable amounts of clays and silt. The dominant carbonate mineral in most marls is calcite, but other carbonate minerals such as aragonite, dolomite, and siderite may be present. In the major element results we see a sharp transition from the primarily, calcium carbonate, Buda Limestone to a more calcareous marl in the Lower Eagle Ford. Going up section the Lower Eagle grades from a calcareous marl to more argillaceous marl. The Middle Eagle Ford contains the high concentrations of clay does and not contain much of continuous carbonate layer. The Upper Eagle Ford is consistently more enriched in calcium carbonate and is only slightly argillaceous.

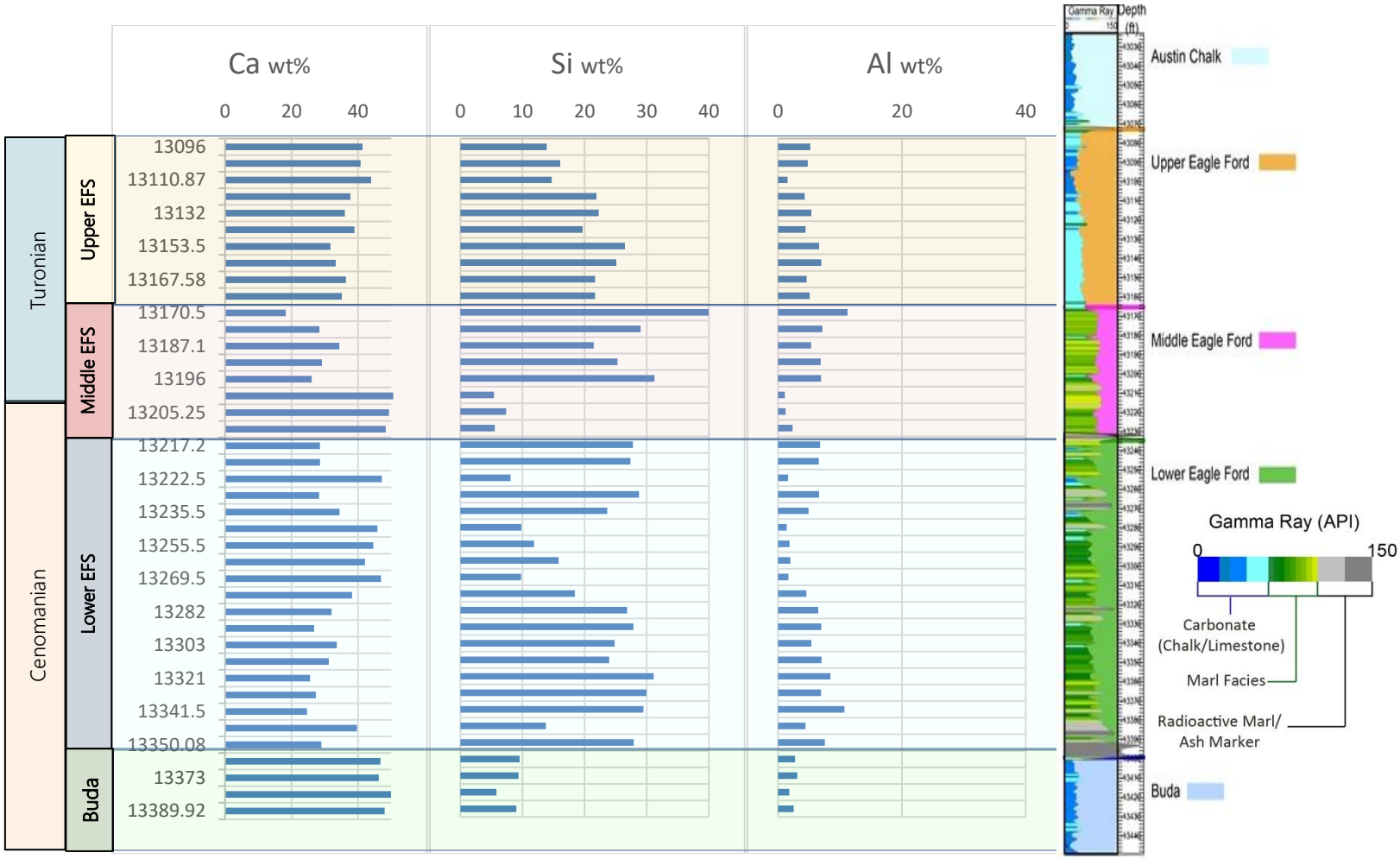

Figure 5.1 Vertical depth profile of major elements compared to gamma ray log API units Modified from Chemostrat Inc.

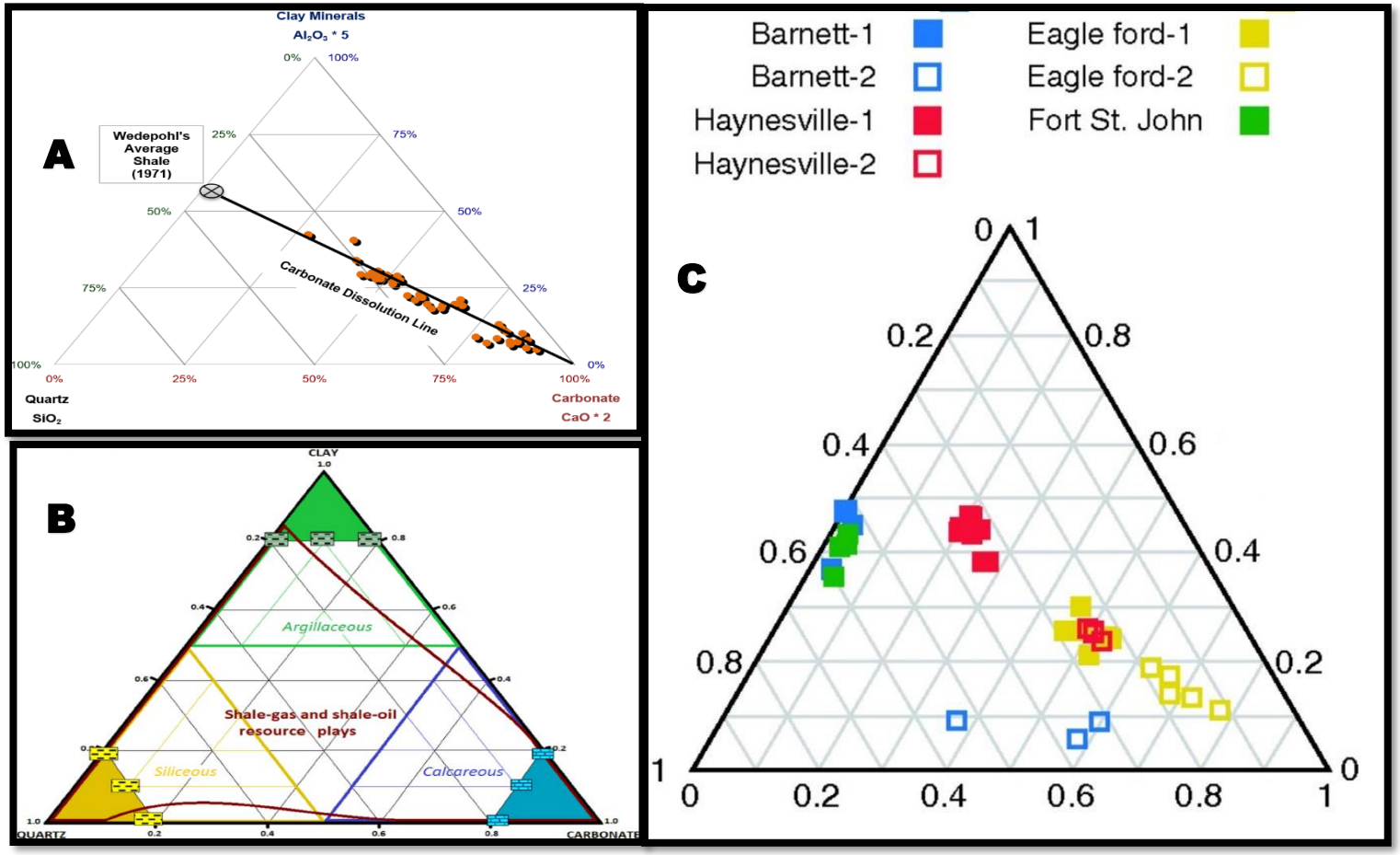

Figure 5.2 **(A)** EFS subsurface core from this study. **(B)** Generalized ternary diagram Modified from (Valdiviezo-Mijangos et. Al., 2014). **(C)** Lithological comparison of black shales. Modified from (Sone and Zoback 2013)

The samples taken from the EFS were plotted in a calcite-clay-quartz ternary diagram and compared to other black shales (Figure 5.2). A general trend towards the calcareous end member is shown. Also a strong correlation with previous EFS study by Sone & Zoback (2013), illustrated the inherent calcareous nature of the Eagle Ford compared to other shales in North America (Barnett , Haynesville and Ft. St. John).

Major and trace element concentrations were also plotted relative to Post Australian Archean Shale, PAAS (Taylor and McLennan, 1985), which represents the average continental crust (Figure 5.3). These concentrations were plotted against TOC, $\delta 13C_{org}$ excursion, and Ca/Al (proxy representing eustatic sea level rise and fall). The initiation of OAEII correlates with a strong enrichment in CaO and depletion in all other elements (SiO_2, Al_2O_3, and TiO_2) relative to PAAS. This is possibly due to the major transgression that was defined by the highest Ca/Al value which represents a high carbonate to clay ratio and defined by a maximum flooding surface (MFS). The increase in calcium carbonate could have caused a dilution in the measured values for elements (SiO_2, Al_2O_3, and TiO_2) relative to PAAS. The TOC values also show a strong depletion after the maximum flooding surface is reached at the beginning of OAEII. This depletion in TOC appears to be correlated with a depletion in CaO and enrichment of elements (SiO_2, Al_2O_3, and TiO_2).

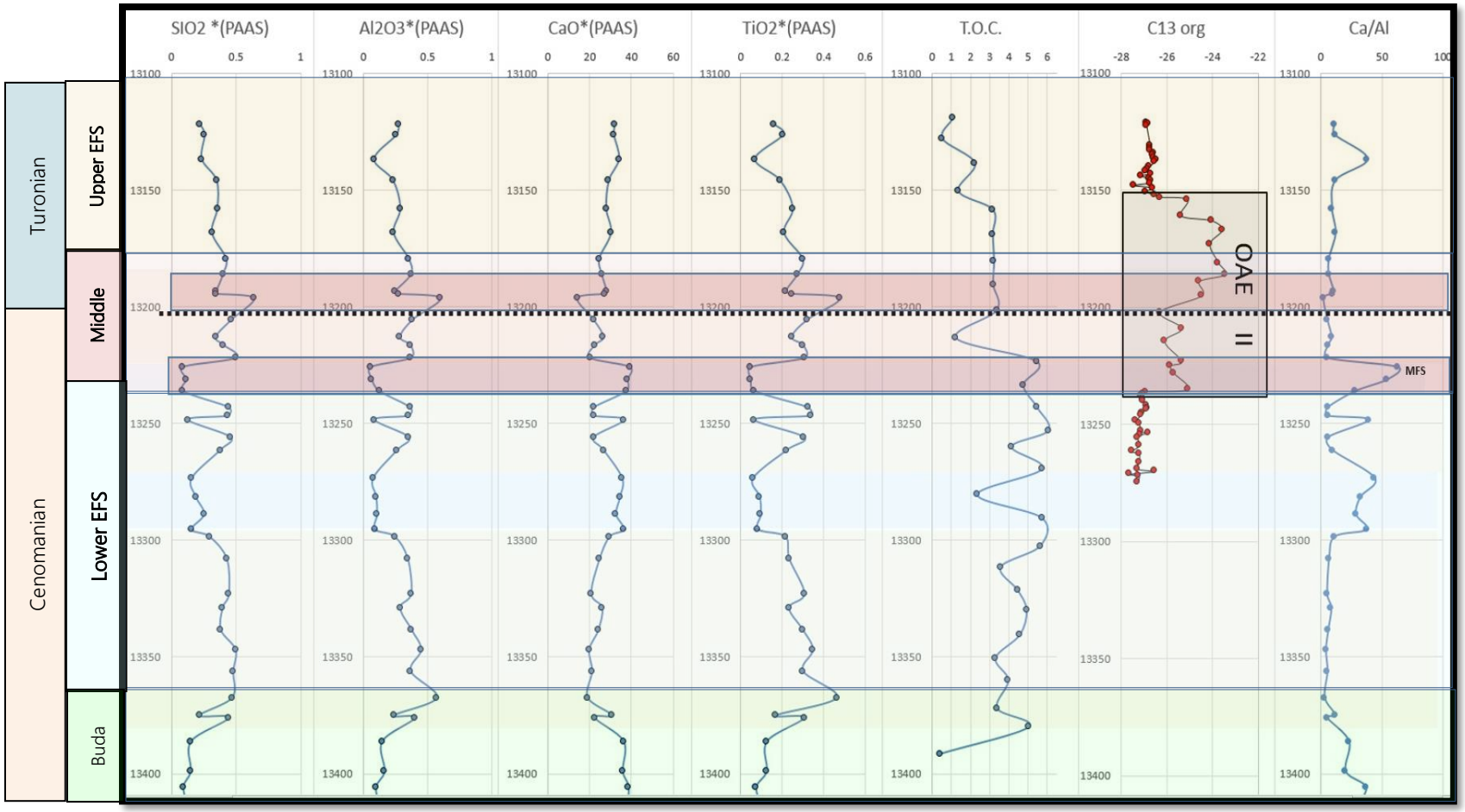

Figure 5.3 Subsurface EFS core element (SiO_2, Al_2O_3, CaO, and TiO_2) concentrations relative to PAAS, compared to TOC, $\delta 13C_{org}$ excursion, and Ca/Al proxy for maximum flooding surface(MFS)

In (Figure 5.3), silicon, calcium, potassium, phosphorus, titanium and iron are all shown relative to aluminum. Aluminum can be used as a proxy for the clay and silt content of the core to quantify the mixed marl formation. The linear trends represent the relationship of the element to aluminum and non-linear trends indicate a lack of correlating relationship.

The elements silicon, potassium and titanium also show linear trends for the core. These trends indicate Si, K and Ti are associated with a clay mineral phase. Any deviations, above the linear trend in silicon, indicate enrichment of silica in possible detrital or biogenic quartz form. There are not many deviations above the linear trend in titanium, indicate the titanium is likely not enriched in another form of TiO_2, like rutile which has been found in the EFS. The deviations above the trend in potassium indicate the presence of another mineral phase, possibly K-feldspar ($KAlSi_3O_8$). The phosphorus shows little to no trend indicating no correlations or relationships to the clay fraction of the subsurface sediments. The presence of a negative slope of the calcium relative to the aluminum indicates the clay content was likely diluted by calcium deposition.

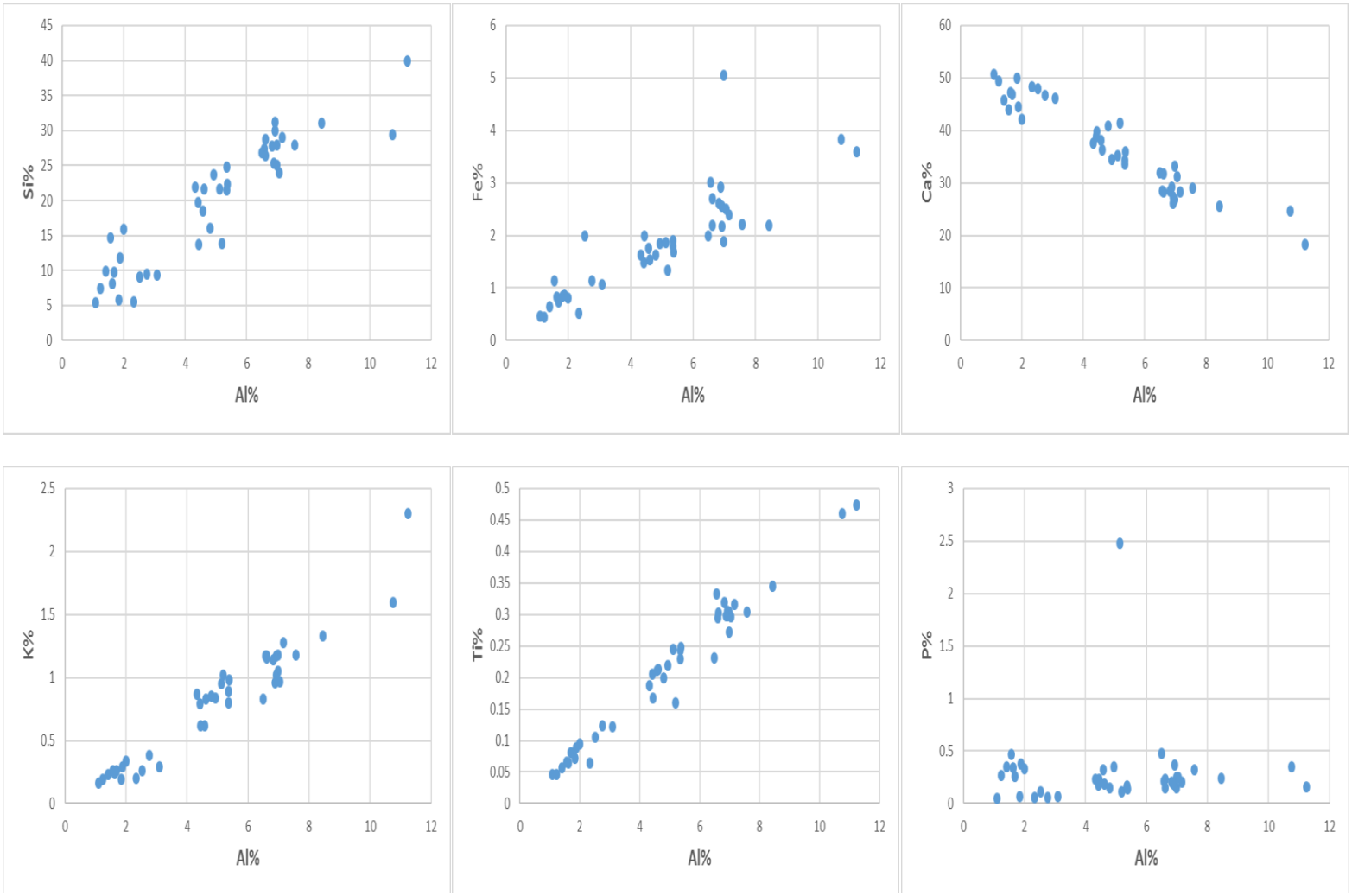

Figure 5.4 General trends of aluminum (clay) enrichment relative to major element elements, values expressed in Wt%.

In (Figure 5.4) the element sulfur is shown relative to iron. This comparison recognizes that the sulfur atoms in pyrite occur in pairs with clear S–S bonds. Pyrite is best described as $Fe^{2+}S_2^{2-}$. These persulfide units can be viewed as derived from hydrogen disulfide, H_2S_2. Thus pyrite would be more descriptively called iron persulfide, not iron disulfide. Sulfur and iron show a strong relationship throughout the core which is indicative of a pyrite (FeS2) association and supported by the fact that pyrite nodules are present throughout the core.

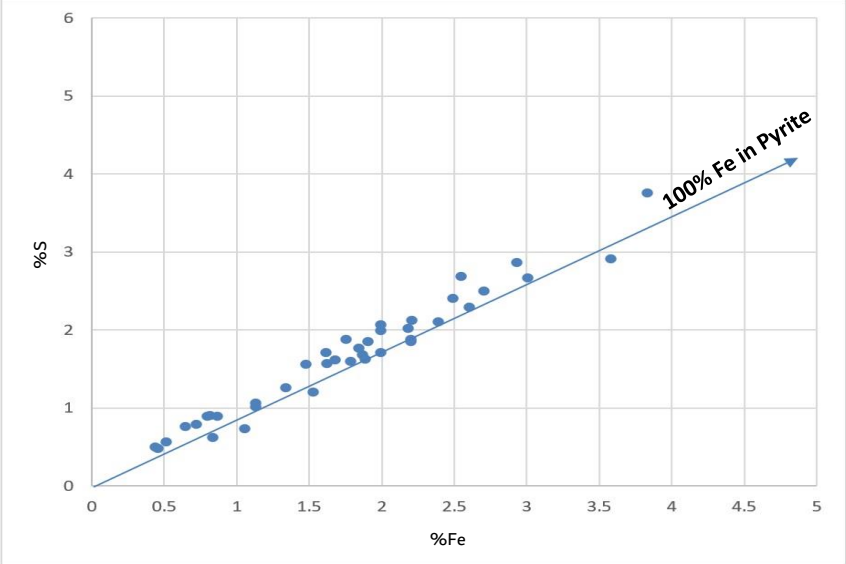

Figure 5.5 Graph of pyrite line with sulfur shown relative to iron (Modified from Raiswell & Berner, 1985).

5.1.3 Minor and Trace Element Interpretation compared with TOC and $\delta^{13}C_{org}$

Analysis of the subsurface EFS core samples show an ~80-99% increase in abundance of Co, Cr, Cu, Ni, Mo, Zn over the average Post Australian Archean Shale(PAAS), representative of average continental crust (Figure 5.6). The first volcanogenic-rich interval reached peak values before the onset of OAE2 (Figure 5.7).

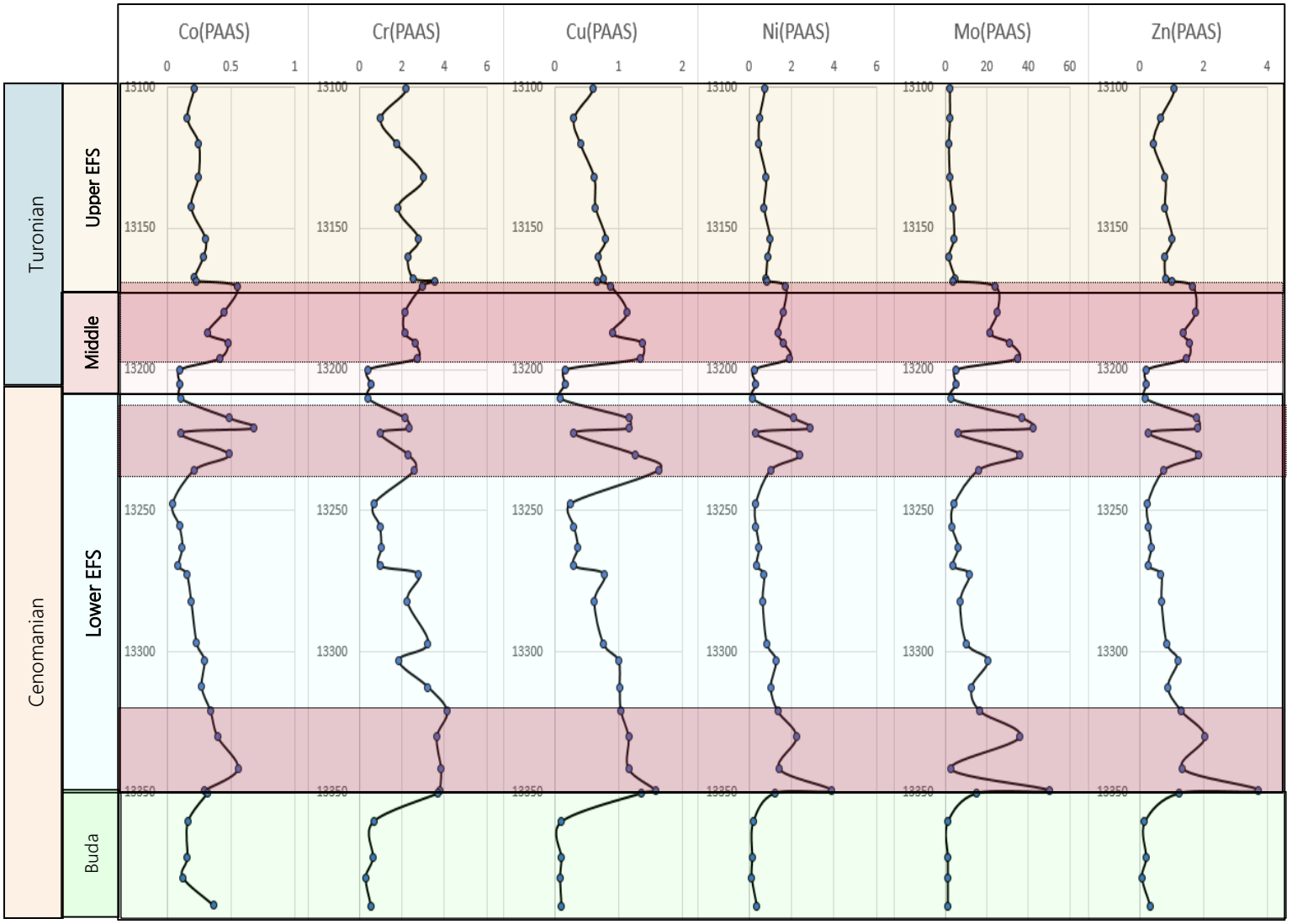

Figure 5.6 Subsurface EFS core Minor and Trace element (Co, Cr, Cu, Mo, Ni V and Zn) concentrations in ppm normalized to Post Australian Archean Shale(PAAS). Enrichment compared average continental crustal values.

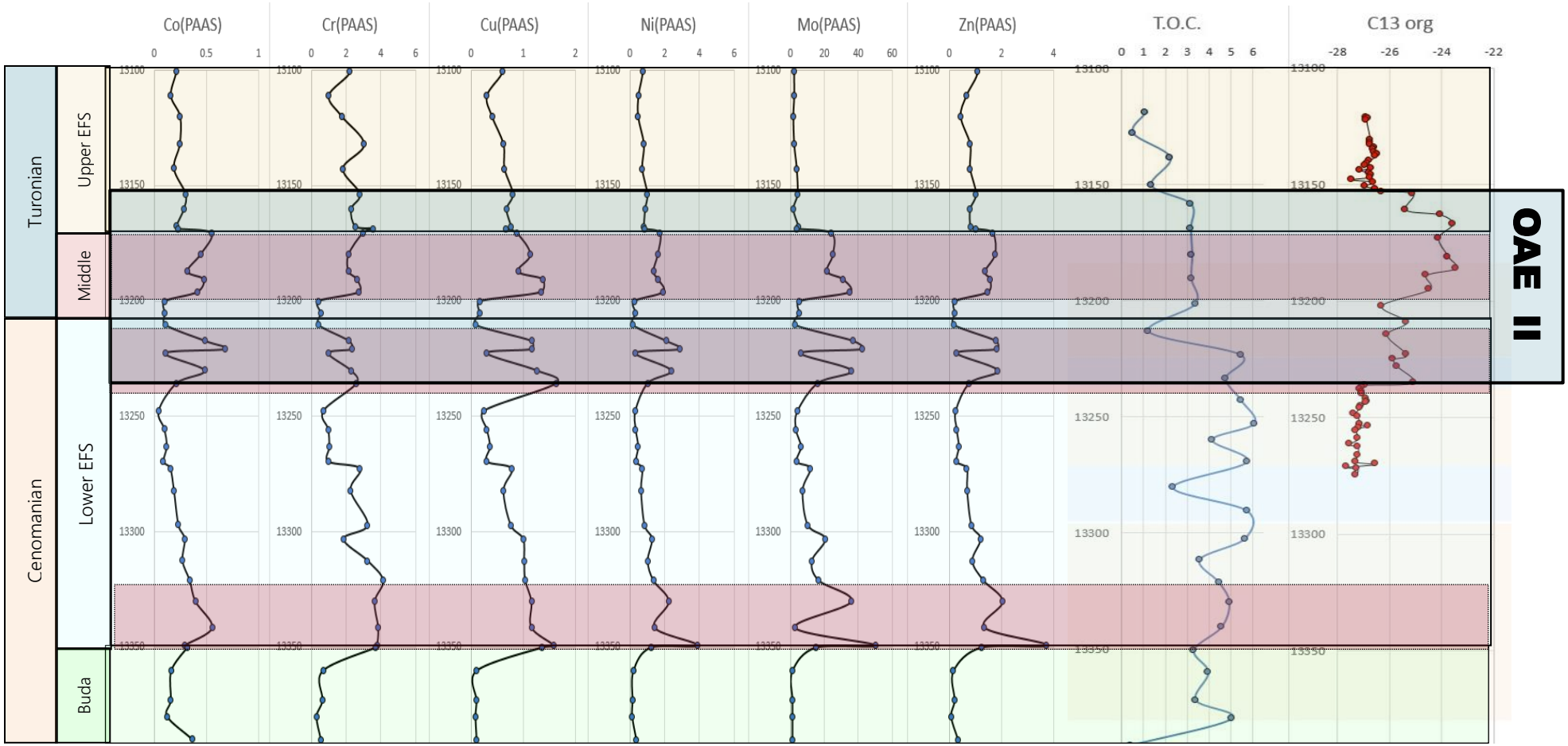

Figure 5.7 Subsurface EFS core Minor and Trace element (Co, Cr, Cu, Mo, Ni V and Zn) concentrations in ppm normalized to Post Australian Archean Shale(PAAS) and compared to TOC and $\delta^{13}C_{org}$ positive excursion (OAEII)

5.1.4 Redox, Paleoproductivty Nutrients and Paleodepositional Proxies

The graphs and cross plots are normalized to enrichment factors (EFs) relative to aluminum. The formula is listed below:

EF = (element in ppm/Al in ppm)sample / (element in ppm/Al in ppm)standard

Elements were normalized over Al primarily because Al is conservative and stable and estimates the “background” contribution of an element derived from crustal sources (Calvert and Pedersen, 2007). Al is abundant in weathering profiles and is present due to the in situ formation of clay minerals and its mechanical erosion from continental rocks, which eventually are transported onto the sea floor (Calvert and Pedersen, 2007).

Redox sensitive trace metals tend to be soluble under oxic conditions and less soluble under reducing conditions, which explains why certain trace metals are authigenically enriched in oxygen-depleted facies (Tribovillard et al., 2006).

Trace metals are either present in seawater in a soluble form or can be adsorbed onto particles. Under reducing conditions metallic ions of elements are adsorbed onto organic material, can form organometallic complexes, or precipitated as iron sulfides (Tribovillard et al., 2006).

A proxy for trace metal deposition onto continental shelves and the subsequent development of an oxygen minimum zone (OMZ) was suggested by Brumsack (2006). The primary producers, planktonic blooms, occur cyclically when there is renewed availability of nutrients including trace metals in the water column they live in (Brumsack, 2006).

The elemental concentrations are plotted against total organic content (%TOC) and δ13Corg positive excursion to correlate redox, nutrient and upwelling proxies to the organic rich black shale of the EFS of south Texas (Figure 5.8).

Molybdenum concentrations are highest in the middle and lower Eagle Ford showing mainly anoxic bottom water conditions during Eagle Ford time in this south Texas location. Phosphorus tends to show a correlation with upwelling. The positive EFs of molybdenum, nickel, copper and zinc, and are mostly coincident with each other showing a sharp increase immediately after the Buda Limestone and at the transition between the Lower and Middle EFS.

These organic proxies represent the nutrients available during the deposition of the EFS subsurface core. Phosphorus is enriched in most all settings, however there is a greater degree of enrichment in an upwelling environment. Iron is enriched in an upwelling environment but shows a general depletion up section after the Lower EFS maximum. possible correlating to the Lower EFS transition from the Buda. However it becomes depleted up section. Fe can be a nutrient but it is mainly concentrated in clastic rocks (Calvert and Pedersen, 2007), which is why it could be depleted in the Eagle Ford relative to average shale. Mn is depleted in the Eagle Ford as well as in the equivalent of an upwelling environment, yet it is slightly more enriched in this location.

The δ13Corg positive isotope excursion appears to correlate with the enrichment of nutrient proxies (Ni, Cu, Zn). The excurison also shows a correlation with Mo which suggest anoxic conditions after the onset of OAEII.

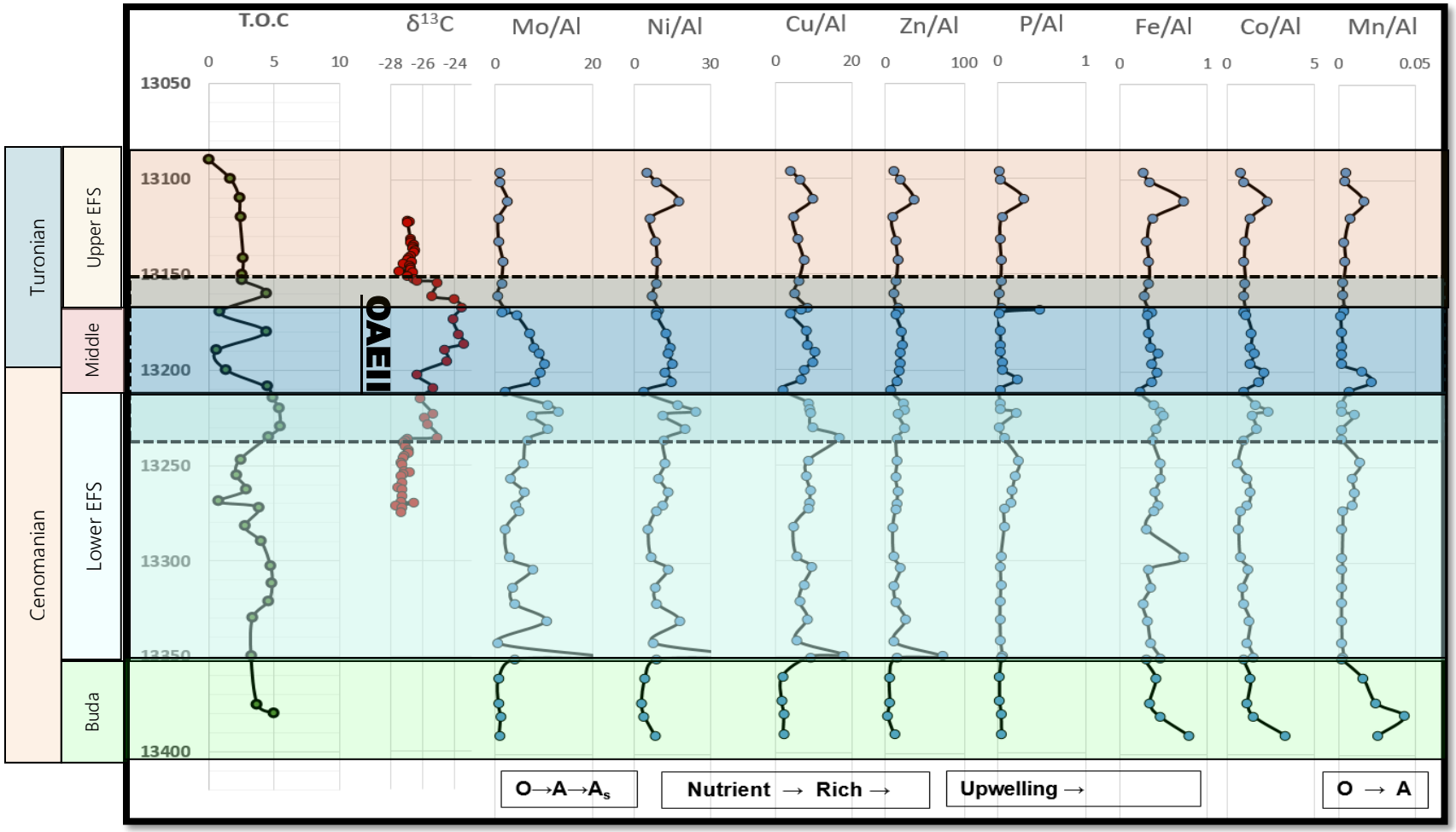

Figure 5.7 Subsurface EFS core redox, nutrient and upwelling proxies compared to TOC and $\delta^{13}C_{org}$ positive excursion (OAEII)

Figure 5.8 from Brumsack (2006) illustrates the sediment capture of trace metals under an anoxic water column with high productivity at the sea surface above an extended shelf which experiences upwelling (idealized conditions for the shallow marine environment of EFS of South Texas). The sporadic H2S in the water column is present as a byproduct of oxygen consumption by microbial organisms (sulfur-reducing bacteria) as decaying organic matter is oxidized or as they reduce excess inorganic sulfate into sulfide (e.g., Barton and Fauque, 2009).

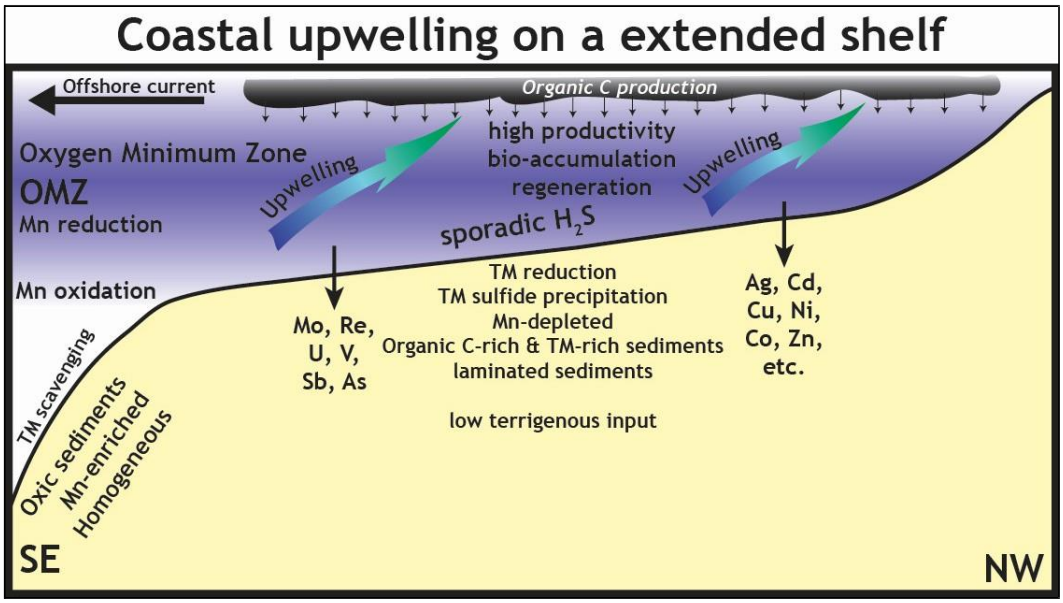

Figure 5.8 Trace metals are captured into sediment when they come out of solution under anoxic conditions when free H_2S is present within the water column and form sulfides. The ocean surface productivity is a result of nutrient input and a cyclical supply of oxygen by upwelling of bottom waters. Modified from Brumsack (2006).

Chapter 6

CONCLUSIONS

6.1 Conclusions and Future Work

Major, minor and trace elements, integrated with stable isotope, organic carbon and geochronological data, were used to characterize three stratigraphic facies (Upper, Middle and Lower), identify volcanically enriched horizons and get an absolute date for the inferred CT boundary of the ~300ft subsurface core of the Eagle Ford Formation of south Texas.

The Eagle Ford Shale of South Texas showed multiple depositional environments evident from the major elemental analysis. The lower Eagle Ford grades from the calcium carbonate limestone at the unconformable contact with Buda formation to a calcareous marl before transitioning to a more argillaceous marl. The middle Eagle Ford grades from a slightly argillaceous limestone to a predominantly calcareous mudstone, evident from the highest concentrations of clay seen directly before the transition to the upper Eagle Ford. The upper Eagle Ford is consistently more enriched in calcium carbonate and is only slightly argillaceous.

Geochemical proxies suggest the Eagle Ford Formation was deposited in a continuously evolving shallow marine environment ranging from inner to outer shelf with a partially restricted basin during eustatic sea level changes which is suggested through the anoxic/euxinic, sub-oxic and oxic changes. Open marine conditions show higher calcium carbonate while more restricted environments show less. Five major transgressive events have been described in the Cretaceous Western Interior Seaway. The most prominent is transgressive event being associated with the initiation of the OAEII and C/T boundary. This maximum transgressive event is represented through the

Ca/Al peak which shows the maximum transgressive high stand carbonate deposition in the EFS. As previously stated, this suggest the eustatic transgressive sea level rise and consequential maximum flooding surface, played a role in depleting the otherwise enriched signal of volcanogenic elements seen pre and post OAEII. The volcanically enriched horizons likely were continuous throughout the entire OAEII and eustatic transgressive sequences decreased the ability for the elements to be preserved after their deposition.

The stable isotope $\delta^{13}C_{org}$ positive excursion directly correlates with the initiation of OAEII in the middle EFS. The dated zircons from the bentonite bed directly above the inferred C/T boundary are shown to agree well with biostratigraphically determined age of 95.9-93.7Ma, with a chronostraigraphically determined U-Pb dated age of 93.2 ±1.7 Ma. Using these ages as a geochronological parameter(datum), the onset of OAEII can be constrained and correlated to the positive carbon ($\delta^{13}C$) isotope excursion to a high degree of certainty.

Trace element data integrated with the $\delta^{13}C_{org}$ and the dated zircons suggested intervals of significantly increased volcanogenic trace metal input correlating to increased organic matter, and a slight increase in ($\delta^{18}O$) at the C/T boundary. The onset of the Carbon ($\delta^{13}C$) excursion first appears ~60ft before the dated zircons and shows an initial ~2% increase from -27.05% to -25.09%. At approximately one ft. above the C/T dated bentonite bed we see a secondary ~3% increase from -26.31% to -23.45% over a 10ft interval for $\delta^{13}C$ values correlating with increased volcanic trace metal signature. OAEII, defined by the positive carbon ($\delta^{13}C$) isotope excursion, was found to span over an interval of ~85ft from (13236-13154 ft.). This well-defined OAEII interval was analyzed at a higher resolution using ED-XRF. Samples were taken at ~6 to 10 in intervals throughout the C/T OAE2 defined by the ($\delta^{13}C$) isotope excursion and show intervals of

(80-99%) increase in trace elements (i.e. Cr, Cu, Ni, Mo, Zn). These intervals reach peak values before the onset of OAEII, and could be responsible for magmatic-induced bottom water anoxia and increase levels of organic carbon preservation at or before the onset of the C/T transition boundary. A possible source could have been Caribbean oceanic plateau, a Large Igneous Province (LIP) which has been previously studied and suggest the rapid flood basalt volcanism initiated ~90Ma and may have preceded the onset. The presence of intermittent bentonite beds deposited throughout the core suggest volcanism throughout the formation from a relatively nearby source. The small size of the zircons grains suggest volcanic ash fall with previous studies of EFS bentonite beds confirming a volcanic arc origin for the weather ash beds found intermittently throughout the region. Volcanic gas output may have also influenced the acidification of the oceans during OAEII and caused the mass extinction at the C/T boundary resulting in the deposition of significant amounts of organic rich black shale. The exact source of the Eagle Ford volcanic material is uncertain and requires further study.

Contemporaneous volcanism through the Eagle Ford was known to be occurring west of the KWIS from the magmatic arc formation comprised from the Sevier Orogeny. The combined influences from LIP flood basalt eruptions and regional volcanism may have affected paleodepositional water conditions and possibly inputted excess CO_2 input into the oceans and atmosphere resulting in the acidification of the oceans from being unable to remove excess gas from the atmosphere. Although the exact cause of the marine anoxia, OAEII, during the Late Cretaceous remains uncertain, the characterization of this ~300ft subsurface core helps support the global contemporaneous deposition of the black shale seen in the Eagle Ford Formation. Understanding the geochemical signatures leading up to global perturbations is

necessary to help further explain the mechanism or trigger involved to cause an even like the OAEII and C/T boundary event.

Appendix A

Elemental Data Tables

University of Texas at Arlington Department of Geology

Light Stable Isotope Lab

Stable Isotope $\delta^{13}C_{org}$ acquired by the Costech ECS 4010 elemental analyzer interfaced with a Thermo Finnigan Conflo IV device to a Thermo Finnigan Delta-V isotope-ratio mass spectrometer (IRMS).

Depth	$\delta^{13}C_{org}$		Depth	$\delta^{13}C_{org}$		Depth	$\delta^{13}C_{org}$
13122.4	-26.9066		13153	-26.3		13240	-27.0517
13131	-26.746		13154	-25.11		13242	-26.8937
13132.05	-26.758		13161	-25.39		13243	-26.8493
13133	-26.765		13163	-24.06		13243.5	-26.8953
13134	-26.582		13167	-23.58		13245	-27.1103
13135	-26.645		13173	-24.13		13246	-27.1593
13136	-26.595		13181	-23.75		13248.5	-27.3663
13137	-26.453		13186	-23.45		13249.5	-27.2363
13138	-26.56		13189	-24.6		13253	-27.1263
13140	-26.773		13195	-24.47		13253.5	-26.8223
13141	-26.848		13202	-26.31		13254.5	-27.1923
13142	-26.933		13209	-25.36		13255.5	-27.3143
13142.98	-26.692		13214.5	-26.12		13259	-27.2233
13143.98	-27.148		13223	-25.36		13261.5	-27.5545
13144.99	-26.784		13225	-25.86		13262.5	-27.2365
13146	-26.719		13228	-25.72		13266	-27.2395
13147	-26.761		13235	-25.09		13269	-27.2925
13148	-27.465		13236	-26.9277		13270	-26.5635
13149	-26.643		13237	-27.0657		13271.2	-27.6435
13150.7	-26.935		13238	-27.1427		13272	-27.2435
13152	-26.54		13239	-27.0757		13274.5	-27.2945

University of Texas at Arlington Department of Geology

Shimadzu Center for Environmental, Forensics and Material Science

Energy Dispersive X-ray Fluorescence (ED-XRF) Data

Depth	Cr		Ni		Cu		Zn		Mo
13090	7.7	13090	13.7	13090	31.6	13090	33.1	13090	14.5
13100	22.1	13100	44.8	13100	32.4	13100	23.2	13100	3.1
13110	22.5	13110	49.6	13110	42.8	13110	116.3	13110	3.1
13120	29.2	13120	50.5	13120	33.6	13120	95.2	13120	5.7
13123	54.6	13123	187.7	13123	43.5	13123	117.1	13123	47.4
13132	29.5	13132	29.2	13132	33.9	13132	9	13132	2.6
13142	23.3	13142	40.9	13142	35.2	13142	46.6	13142	4.2
13150	22.4	13150	23.4	13150	30.9	13150	11.3	13150	2.2
13153	18.4	13153	27.1	13153	34.9	13153	3.5	13153	3.1
13160	28.2	13160	34.9	13160	36.3	13160	30.3	13160	4.3
13165	29.9	13165	45.6	13165	25.8	13165	43.5	13165	4.1
13166	25.6	13166	49.5	13166	24.4	13166	22.7	13166	3.7
13167	20.4	13167	36.1	13167	20.1	13167	34.3	13167	3.5
13168	25.7	13168	32.1	13168	25.4	13168	27.8	13168	3.1
13169	2.9	13169	76.2	13169	6.8	13169	2.2	13169	2.4
13170	81.3	13170	71.5	13170	35.7	13170	55.5	13170	34.1
13171	360.9	13171	34.5	13171	39.3	13171	6.7	13171	26.5
13172	6.3	13172	54.9	13172	26.9	13172	0	13172	3.4
13174	17.7	13174	26	13174	31.1	13174	13.3	13174	8.7
13175	36.1	13175	44.8	13175	37.1	13175	116.5	13175	17.5
13196	52.4	13196	135	13196	45.3	13196	93.9	13196	40.8
13198	57.2	13198	115.4	13198	45	13198	69.5	13198	37.8
13199	50.1	13199	135.2	13199	43.9	13199	93.3	13199	38.3
13200	4.9	13200	77.8	13200	27.3	13200	0	13200	3.9
13201	53.2	13201	145.4	13201	46.1	13201	97.3	13201	50.1
13202	48.2	13202	160.4	13202	43	13202	104.9	13202	46.4
13203	65.1	13203	180.2	13203	44.1	13203	101.5	13203	53
13204	72.5	13204	216.5	13204	48.7	13204	142.6	13204	58.1
13205	41.7	13205	66.4	13205	38	13205	43.7	13205	26.3
13206	52.8	13206	116.4	13206	40.6	13206	53.4	13206	34.9
13207	8.4	13207	58.6	13207	27.9	13207	0	13207	5.1
13208	46.3	13208	110.3	13208	37.5	13208	104.2	13208	32.7
13209	42.3	13209	114.5	13209	37.2	13209	95.5	13209	31.2
13210	5.9	13210	58.6	13210	8.1	13210	6.1	13210	3.9
13211	73.4	13211	151.8	13211	46.9	13211	116.5	13211	48.2

13213	6.4	13213	60.4	13213	26.6	13213	0	13213	4.2
13214	7.6	13214	55.4	13214	28.1	13214	0	13214	5.3
13215	48.6	13215	118	13215	41.5	13215	91.8	13215	36.9
13216	43.7	13216	152.2	13216	34.7	13216	146.3	13216	37
13220	53.4	13220	182.4	13220	43.5	13220	102.2	13220	49.8
13235	48.4	13235	105.7	13235	49.1	13235	65	13235	34.7
13247	10	13247	39.5	13247	33	13247	0	13247	4.7
13255	7.8	13255	41.7	13255	29.8	13255	0	13255	3.7
13263	37.4	13263	39	13263	36.9	13263	0	13263	7.8
13269	9.6	13269	53.5	13269	27.3	13269	0	13269	2.5
13272	50	13272	51	13272	40.7	13272	21.6	13272	19.7
13282	35.7	13282	26.6	13282	37.4	13282	40.4	13282	12.6
13297	58.2	13297	33.7	13297	40	13297	33.9	13297	11.3
13303	44.3	13303	102	13303	45.4	13303	88.7	13303	41.9
13312	59.5	13312	47.8	13312	46.6	13312	43.2	13312	16.1
13321	59.5	13321	65.8	13321	39.4	13321	41.4	13321	23.1
13330	39.5	13330	74.2	13330	39	13330	41.1	13330	31.9
13340	54.9	13340	53.9	13340	38.1	13340	72.4	13340	6.5
13342	89.5	13342	75.2	13342	43.5	13342	119.6	13342	8.9
13343	79	13343	74.9	13343	41.5	13343	96.4	13343	7.1
13344	76.9	13344	85.5	13344	42.4	13344	106.2	13344	7
13346	107.2	13346	128.3	13346	46.6	13346	149.7	13346	9.3
13347	90.9	13347	126.3	13347	42.3	13347	73.7	13347	8.9
13348	121	13348	95.7	13348	43.5	13348	0	13348	16.9
13349	129.9	13349	134.5	13349	43.7	13349	159.9	13349	18.8
13350	84.3	13350	112.5	13350	45.3	13350	185.2	13350	29.6
13351	6.6	13351	52.5	13351	27.3	13351	0	13351	3
13352	36.2	13352	73.7	13352	33.1	13352	49.7	13352	4.3
13353	233.4	13353	59.4	13353	37.8	13353	40.5	13353	13.4
13354	107.7	13354	129.9	13354	43.4	13354	148.1	13354	18.1
13356	104.2	13356	118.8	13356	42.1	13356	128.5	13356	51.8
13357	81.1	13357	77.2	13357	40.5	13357	102.8	13357	14.6
13358	114.5	13358	173.9	13358	51.1	13358	182.2	13358	59.3
13359	71.1	13359	116.2	13359	47.2	13359	161.4	13359	12.1
13360	147.1	13360	250.1	13360	53.5	13360	236.5	13360	83.9

University of Texas at Arlington Department of Geology

Shimadzu Center for Environmental, Forensics and Material Science

Total Organic Carbon Analyzer TOC-V with Solid Sample Module SSM-5000A

CLB Depth	T.O.C.
13080	1.13
13094.5	1.1
13104.5	0.52
13114.5	2.22
13126.5	1.36
13134.5	3.17
13145	3.16
13154.5	3.22
13164.5	3.18
13174.5	3.37
13187.5	1.24
13197.5	5.47
13208	4.76
13217.5	5.47
13227.5	6.08
13234.5	4.14
13244.5	5.74
13254.5	2.34
13266	5.73
13276.5	5.64
13286.5	3.57
13296.5	4.47
13305	4.93
13316	4.58
13326	3.3
13334.5	3.97
13346.5	3.38
13354.5	5.03
13365.5	0.4

University of Texas at Austin, Department of Geological Science

The Analytical Laboratory for Paleoclimate Studies (ALPS)

Thermo Electron Kiel IV automated carbonate device connected to a Thermo Electron MAT253 or Delta V dual inlet isotope ratio mass spectrometer (IRMS),

δC^{13}_{carb}	Depth		δO^{18}	Depth
-0.28738	13132		-6.49	13132
-0.81044	13142.5		-6.20	13142.5
0.300309	13153.5		-6.47	13153.5
-0.13027	13160.08		-6.42	13160.08
0.073586	13167.58		-6.27	13167.58
0.254566	13168.58		-6.60	13168.58
0.287382	13170.5		-6.45	13170.5
0.20783	13179.75		-6.50	13179.75
-0.04674	13187.1		-6.31	13187.1
-0.01094	13190.5		-6.42	13190.5
0.242634	13196		-6.43	13196
-2.80918	13200		-3.77	13200
0.306275	13205.25		-6.33	13205.25
0.095462	13210.25		-4.55	13210.25
0.912859	13217.2		-6.49	13217.2
0.930758	13220.75		-6.58	13220.75
0.835296	13235.5		-6.45	13235.5
0.876066	13247.5		-5.25	13247.5
1.991783	13255.5		-5.43	13255.5
-0.23567	13263		-5.77	13263
1.813786	13269.5		-5.23	13269.5
0.035798	13282		-5.02	13282
1.231067	13297		-6.32	13297
0.838279	13303		-6.26	13303
0.46339	13312.5		-5.84	13312.5
0.611556	13330.17		-6.13	13330.17
1.388182	13341.5		-5.24	13341.5
0.988434	13349.08		-6.11	13349.08
0.193908	13350.08		-5.58	13350.08
1.544303	13373		-4.42	13373

References

Algeo, T.J., Maynard, J.B., 2004, Trace-element behavior and redox facies in core shales of Upper Pennsylvanian Kansas-type cyclothems, Chemical Geology, v. 206, is. 3-4, p. 289-318.

Algeo, T.J., Lyons, T.W., Mo-total organic carbon covariation in modern anoxic marine environments: implications for analysis of paleoredox and paleohydrographic conditions, Paleooceanography, v. 21, p. 1-23.

Algeo, T.J., Heckel, J.B., Maynard, Blakey, R., Rowe, H., 2008, Modern and ancient epicratonic seas and superestaurine circulation model of marine anoxia, in Holmden and BR Prat, (Eds). Dynamics of Epeiric Seas, Paleontological and Geochemical Perspectives: Geological Association of Canada Special Publication, Vol. 48, p. 7-38.

Algeo, T.J., Tribovillard, N., 2009, Environmental analysis of paleoceanographic systems based on molybdenum-uranium covariation, Chemical Geology, v. 268, p. 211-225.

Algeo, T.J., Rowe, H., 2012, Paleoceanographic applications of trace-metal concentration data, Chemical Geology, v. 324-325, p. 6-18.

Arthur, M.A., Dean, W.E., Pratt, L.M., 1988, Geochemical and climatic effects of increased marine organic carbon burial at the Cenomanian/Turonian boundary: Nature, v. 335, p. 714-717.

Arthur, M.A. and Sageman, B.B., 1994, Marine Black Shales: Depositional Mechanisms and Environments of Ancient Deposits: Annual Reviews of Earth Planetary Science, v. 22, p. 499-551.

Arthur, M.A. and Schlanger, S.O., 1979, Cretaceous "Oceanic Anoxic Events" as Causal Factors in Development of Reef-Reservoired Giant Oil Fields, The American Association of Petroleum Geologists Bulletin, v. 63, vo. 6. p. 870-885.

Arthur, M.A., Schlanger, S.O., Jenkyns, H.C. 1987, The Cenomanian-Turonian oceanic anoxia event: II. Paleoceanographic controls on organic matter production and preservation. Geological Society, London, Special Publications, Vol. 26, p. 401-420.

Berner, R.A., and Raiswell, R., 1983, Burial of organic carbon and pyrite sulfur in sediments over Phanerozoic time: a new theory: Geochemica et Cosmochimica Acta, Vol. 47, Issue 5, p. 855-862.

Blakey, R., 1994, Global Paleogeography, Northern Arizona University. <http://www2.nau.edu/rcb7/nam.html>, Accessed November, 2014.

Brown, C.W., and Pierce, R.L., 1962, Palynologic correlations in Cretaceous Eagle Ford Group, northeast Texas: American Association of Petroleum Geologists Bulletin, v. 46, p. 21332147.

Bodziak, Robert, et al. "The Role of Seismic Attributes in Understanding the Hydraulically Fracturable Limits and Reservoir Performance in Shale Reservoirs: An Example from the Eagle Ford Shale, South Texas." *AAPG Bulletin* 98.11 (2014): 2217-35.

Brumsack, Hans-J. "The Trace Metal Content of Recent Organic Carbon-Rich Sediments: Implications for Cretaceous Black Shale Formation." *Palaeogeography, Palaeoclimatology, Palaeoecology* 232.2 (2006): 344-61.

Caldeira, Ken, and Michael R. Rampino. "The Mid-Cretaceous Super Plume, Carbon Dioxide, and Global Warming." *Geophysical Research Letters* 18.6 (1991): 987-90.

Calvert, S.E., 1987, Oceanographic controls on the accumulation of organic matter in marine sediments. Geological Society, London, Speical Publications, v. 26, 137-151.

Calvert, S.E., Pedersen, T.F., 1993, Geochemistry of recent oxic and anoxic marine sediments: implications for the geological record. Marine Geology.v. 113, p 67-88.

Coccioni, R., Galeotti, S., 2003. The mid-Cenomanian Event: prelude to OAE 2, Palaeogeography, Palaeoclimatology, Palaeoecology, v. 190. p. 427-440.

Darmaoen, Shariva Tr. "Major, Minor and Trace Element Geochemistry of the Eagle Ford Formation, South Texas." (2017)

Dawson, W.C., 1997, Shale microfacies: Limestone microfacies and sequence stratigraphy: Eagle Ford Group (Cenomanian-Turonian) north-central Texas outcrops. Gulf Coast Association of Geological Societies Transactions, v. 47, p. 99-105.

Dawson, W.C., 2000. Shale microfacies: Eagle Ford Group (Cenomanian-Turonian) northcentral Texas outcrops and subsurface equivalents: Gulf Coast Association of Geological Societies Transactions, v. 50, p. 607-621.

Dean, W.E. and Arthur, M.A., 1989. Iron-Sulfur relationships in Organic-Carbon Rich Sequence I: Cretaceous Western Interior Seaway. American Journal of Science, v. 289. p. 708743.

Demaison, GJ, and G. Tn Moore. "Anoxic Environments and Oil Source Bed Genesis." *Organic Geochemistry* 2.1 (1980): 9-31.

Donovan, A.D., and Staerker, T.S., 2010, Sequence Stratigraphy of the Eagle Ford (Boquillas) Formation in the Subsurface of South Texas and Outcrops of West Texas: Gulf Coast Association of Geological Societies Transactions, v. 60, p. 861-899.

Du Vivier, Alice DC, et al. "Marine 187 Os/188 Os Isotope Stratigraphy Reveals the Interaction of Volcanism and Ocean Circulation during Oceanic Anoxic Event 2." *Earth and Planetary Science Letters* 389 (2014): 23-33.

Erbacher, Jochen, et al. "Increased Thermohaline Stratification as a Possible Cause for an Ocean Anoxic Event in the Cretaceous Period." *Nature*409.6818 (2001): 325-7.

Friedrich, Oliver, Richard D. Norris, and Jochen Erbacher. "Evolution of Middle to Late Cretaceous oceans—a 55 My Record of Earth's Temperature and Carbon Cycle." *Geology* 40.2 (2012): 107-10.

Gale, A.S., Voight, S., Sageman, B.B., Kennedy, W.J., 2008, Eustatic sea-level record for the Cenomanian (Late Cretaceous)-Extension to the Western Interior Basin, USA, Geology, v. 36, p. 859-862.

Gehrels, George, Victor Valencia, and Alex Pullen. "Detrital Zircon Geochronology by Laser-Ablation Multicollector ICPMS at the Arizona LaserChron Center." *The Paleontological Society Papers* 12 (2006): 67-76. Web.

Hammes, Ursula, et al. "Regional Assessment of the Eagle Ford Group of South Texas, USA: Insights from Lithology, Pore Volume, Water Saturation, Organic Richness, and Productivity Correlations." *Interpretation* 4.1 (2016): SC125-50. Web.

Harbor, R.L., 2011, Facies Characterization and Stratigraphic Architecture of Organic-Rich Mudrocks, Upper Cretaceous Eagle Ford Formation: MS thesis, University of Texas at Austin. 184 p.

Hentz, T.F., and Ruppel, S.C., 2010, Regional lithostratigraphy of the Eagle Ford Shale: Maverick Basin to East Texas Basin: Gulf Coast Association of Geological Societies Transactions, v. 60, p 325-337.

Hentz, T.F., and Ruppel, S.C., 2011, Regional Stratigraphic and Rock Characteristics of Eagle Ford Shale In Its Play Area: Maverick Basin to East Texas Basin. AAPG Annual Convention, Houston, Texas 2011. Search and Discovery Article #10325

Hetzel, A., Bottcher, M.E., Wortmann, U.G., Brumsack, H.J., Paleo-redox conditions during OAE2 reflected in Demerara Rise sediment geochemistry (ODP Leg 2070, Palaeogeography, Palaeoclimatology, Palaeoecology, v. 273, p. 302-328

Hill, R.T., 1901, Geography and geology of the Black and Grand Prairies, Texas: USGS 21st Annual Report, pt. 7, 666 p.

Jenkyns, H.C., 1980, Cretaceous anoxic events: from continents to oceans, Journal of the Geological Society of London, v. 137. p. 171-188.

Jenkyns, H.C., 2010, Geochemistry of oceanic anoxic events, Geochemistry, Geophysics, Geosystems, v. 11 p. 1-30.

Jiang, Ming-Jung, 1989, Biostratigraphy and geochronology of the Eagle Ford Shale, Austin chalk, and lower Taylor marl in Texas based on calcareous nannofossils. (Volumes I and II), Phd dissertation, Texas A&M University.

Jenkyns, H.C, and H-J BRUMSACK SO SCHLANGER. "Stratigraphy, Geochemistry, and Paleoceanography of Organic Carbon-Rich Cretaceous Sequences." *Cretaceous resources, events and rhythms: background and plans for research* 304 (1990): 75. Web.

Larson, Roger L., and Elisabetta Erba. "Onset of the Mid-Cretaceous Greenhouse in the Barremian-Aptian: Igneous Events and the Biological, Sedimentary, and Geochemical Responses." *Paleoceanography* 14.6 (1999): 663-78. Web.

Kauffman, E.G., 1977, Cretaceous facies, faunas and paleoenvironments across the western interior basin: The Mountain Geologist, Field guide: North American Paleontological Convention II, 274 p.

Kauffman, E.G., 1984, Paleobiogeography and Evolutionary Response Dynamic in the Cretaceous Western Interior Seaway of North America. Geological Association of Canada Special Paper, 27

Kearns, T.J., 2011, Chemostratigraphy of the Eagle Ford Formation, MS Thesis, University of Texas at Arlington, 254 p.

Keller, G. and Pardo, A., 2005, Age and paleoenvironment of the Cenomanian-Turonian global stratotype section and point at Pueblo, Colorado: Marine Micropaleontology, v. 51, p. 95-128.

Loucks, B.E., Pechier, L., 2006, Boquillas (Eagle Ford) Upper Slope Sediements, West Texas: Out crop Analogs for Potential Shale Reservoirs, GCAGS Annual Convention, AAPG Search and Discovery article #90056

Lowery, Christopher M., et al. "Foraminiferal and Nannofossil Paleoecology and Paleoceanography of the Cenomanian–Turonian Eagle Ford Shale of Southern Texas." *Palaeogeography, Palaeoclimatology, Palaeoecology* 413 (2014): 49-65..

Meyers, P.A., Dunham, K.W., Ho, E.S., 1988, Organic geochemistry of Cretaceous black shales from the Galicia Margin, Ocean Drilling Program Leg 103, Advances in Organic Geochemistry, v. 13, p. 89-96.

Meyers, P.A., 1994, Preservation of elemental and isotopic source identification of sedimentary organic matter, Chemical Geology, v. 114, p. 289-302.

Miller, Kenneth G., et al. "Late Cretaceous Chronology of Large, Rapid Sea-Level Changes: Glacioeustasy during the Greenhouse World." *Geology*31.7 (2003): 585-8. Web.

Milliken, Kitty L., Suzan M. Ergene, and Aysen Ozkan. "Quartz Types, Authigenic and Detrital, in the Upper Cretaceous Eagle Ford Formation, South Texas, USA." *Sedimentary Geology* 339 (2016): 273-88. Web.

Moriya, Kazuyoshi, et al. "Testing for Ice Sheets during the Mid-Cretaceous Greenhouse using Glassy Foraminiferal Calcite from the Mid-Cenomanian Tropics on Demerara Rise." *Geology* 35.7 (2007): 615-8.

Phelps, R.M., 2011, Middle-Hauterivian to Lower-Campanian Sequence Stratigraphy and Stable Isotope Geochemisty of the Comanche Platform, South Texas; Phd Dissertation, The University Of Texas, Austin, Texas, 240 p.

Railroad Commission of Texas, 2012, Eagle Ford Information, <http://www.rrc.state.tx.us/eagleford/index.php#general>, accessed November 2012.

Ohkouchi, Naohiko, Junichiro Kuroda, and Asahiko Taira. "The Origin of Cretaceous Black Shales: A Change in the Surface Ocean Ecosystem and its Triggers." *Proceedings of the Japan Academy, Series B* 91.7 (2015): 273-91.

"The Origin of Cretaceous Black Shales: A Change in the Surface Ocean Ecosystem and its Triggers." *Proceedings of the Japan Academy, Series B*91.7 (2015): 273-91. Web.

Outlook, Annual Energy. "Energy Information Administration." *Department of Energy* 92010.9 (2010): 1-15. Web.

Phelps, Ryan M., et al. "Response and Recovery of the Comanche Carbonate Platform Surrounding Multiple Cretaceous Oceanic Anoxic Events, Northern Gulf of Mexico." *Cretaceous Research* 54 (2015): 117-44. Web.

Sageman, Bradley B., et al. "Multiple Milankovitch Cycles in the Bridge Creek Limestone (Cenomanian-Turonian), Western Interior Basin." (1998).

Schlanger, S.O. and Jenkyns, H.C., 1976, Cretaceous oceanic anoxic events: causes and consequences, Geologie en Mijnbouw, v. 55. p. 179-184.

Scott, R.W., 2010, Cretaceous Stratigraphy, Depositional Systems, and Reservoir Facies of the Northern Gulf of Mexico. Gulf Coast Association of Geological Societies Transactions, v. 60, p. 597-609.

Taylor, Stuart Ross, and Scott M. McLennan. "The Continental Crust: Its Composition and Evolution." (1985)Web.

Tinnin, Beau M., and Shariva TR Darmaoen. "Chemostratigraphic Variability of the Eagle Ford Shale, South Texas: Insights into Paleoredox and Sedimentary Facies Changes." (2016)Web.

Tribovillard, Nicolas, et al. "Trace Metals as Paleoredox and Paleoproductivity Proxies: An Update." *Chemical Geology* 232.1 (2006): 12-32. Web.

Turgeon, Steven C., and Robert A. Creaser. "Cretaceous Oceanic Anoxic Event 2 Triggered by a Massive Magmatic Episode." *Nature* 454.7202 (2008): 323-6. Web.

Verardo, David J., Philip N. Froelich, and Andrew McIntyre. "Determination of Organic Carbon and Nitrogen in Marine Sediments using the Carlo Erba NA-1500 Analyzer." *Deep Sea Research Part A.Oceanographic Research Papers* 37.1 (1990): 157-65. Web.

Wedepohl, K. Hans. "The Composition of the Continental Crust." *Geochimica et Cosmochimica Acta* 59.7 (1995): 1217-32. Web.

Wilson, Paul A., Richard D. Norris, and Matthew J. Cooper. "Testing the Cretaceous Greenhouse Hypothesis using Glassy Foraminiferal Calcite from the Core of the Turonian Tropics on Demerara Rise." *Geology* 30.7 (2002): 607-10. Web.

Biographical Information

Danie Valencia was born and raised in Houston, Texas. After graduating from high school, Daniel obtained a Bachelor of Science degree in Geological Sciences from the University of Texas at Austin in December 2013 with a minor in Information Systems. While attending class he became interested in the research aspect of the geologic field and obtained a position as a undergraduate research assistant at the Bureau of Economic Geology. In January 2014, Daniel entered the Graduate School at the University of Texas at Arlington to pursue a Master of Science in Geology degree. His personal research interests include the origins of black shales; particularly oil and gas bearing formations in Texas. His future plan is to enter into the PhD program and apply GIS techniques to obtain high resolution environmental surveying and monitoring data.